

## Extrapolating continuous vegetation water content to understand sub-daily backscatter variations

Vermunt, P.C.; Steele-Dunne, S.C.; Khabbazan, S.; Judge, Jasmeet; van de Giesen, N.C.

**DOI**

[10.5194/hess-26-1223-2022](https://doi.org/10.5194/hess-26-1223-2022)

**Publication date**

2022

**Document Version**

Final published version

**Published in**

Hydrology and Earth System Sciences

**Citation (APA)**

Vermunt, P. C., Steele-Dunne, S. C., Khabbazan, S., Judge, J., & van de Giesen, N. C. (2022). Extrapolating continuous vegetation water content to understand sub-daily backscatter variations. *Hydrology and Earth System Sciences*, 26(5), 1223–1241. <https://doi.org/10.5194/hess-26-1223-2022>

**Important note**

To cite this publication, please use the final published version (if applicable). Please check the document version above.

**Copyright**

Other than for strictly personal use, it is not permitted to download, forward or distribute the text or part of it, without the consent of the author(s) and/or copyright holder(s), unless the work is under an open content license such as Creative Commons.

**Takedown policy**

Please contact us and provide details if you believe this document breaches copyrights. We will remove access to the work immediately and investigate your claim.



# Extrapolating continuous vegetation water content to understand sub-daily backscatter variations

Paul C. Vermunt<sup>1</sup>, Susan C. Steele-Dunne<sup>1</sup>, Saeed Khabbazan<sup>1</sup>, Jasmeet Judge<sup>2</sup>, and Nick C. van de Giesen<sup>1</sup>

<sup>1</sup>Faculty of Civil Engineering and Geosciences, Delft University of Technology, 2628 CN Delft, the Netherlands

<sup>2</sup>Center for Remote Sensing, Agricultural and Biological Engineering Department, University of Florida, Gainesville, FL 32611, USA

**Correspondence:** Paul C. Vermunt (p.c.vermunt@tudelft.nl)

Received: 11 September 2021 – Discussion started: 17 September 2021

Revised: 19 December 2021 – Accepted: 9 February 2022 – Published: 4 March 2022

**Abstract.** Microwave observations are sensitive to vegetation water content (VWC). Consequently, the increasing temporal and spatial resolution of spaceborne microwave observations creates a unique opportunity to study vegetation water dynamics and its role in the diurnal water cycle. However, we currently have a limited understanding of sub-daily variations in the VWC and how they affect microwave observations. This is partly due to the challenges associated with measuring internal VWC for validation, particularly non-destructively, and at timescales of less than a day. In this study, we aimed to (1) use field sensors to reconstruct diurnal and continuous records of internal VWC of corn and (2) use these records to interpret the sub-daily behaviour of a 10 d time series of polarimetric L-band backscatter with high temporal resolution. Sub-daily variations in internal VWC were calculated based on the cumulative difference between estimated transpiration and sap flow rates at the base of the stems. Destructive samples were used to constrain the estimates and for validation. The inclusion of continuous surface canopy water estimates (dew or interception) and surface soil moisture allowed us to attribute hour-to-hour backscatter dynamics either to internal VWC, surface canopy water, or soil moisture variations. Our results showed that internal VWC varied by 10 %–20 % during the day in non-stressed conditions, and the effect on backscatter was significant. Diurnal variations in internal VWC and nocturnal dew formation affected vertically polarized backscatter most. Moreover, multiple linear regression suggested that the diurnal cycle of VWC on a typical dry day leads to a 2 (HH, horizontally, and cross-polarized) to almost 4 (VV, vertically, polarized) times higher diurnal backscatter variation than the soil moisture

drydown does. These results demonstrate that radar observations have the potential to provide unprecedented insight into the role of vegetation water dynamics in land–atmosphere interactions at sub-daily timescales.

## 1 Introduction

The long heritage of research on remote soil moisture and biophysical parameter retrieval has shown that backscatter is sensitive to dielectric properties of vegetation, which is strongly related to its water content (Konings et al., 2019; Steele-Dunne et al., 2017). For a long time, this sensitivity to vegetation water content (VWC), here defined as the weight of water captured inside the plant material above a square metre of ground ( $\text{kg m}^{-2}$ ), was considered a barrier to soil moisture retrieval. In the last decade however, backscatter sensitivity to VWC has been used for studies on plant hydraulics and water stress in agriculture and ecosystems (e.g. Frolking et al., 2011; Steele-Dunne et al., 2012; Schroeder et al., 2016; Emmerik et al., 2017; Konings et al., 2017; Steele-Dunne et al., 2019; El Hajj et al., 2019).

The increasing temporal and spatial resolution of spaceborne radar observations creates opportunities for more detailed and extensive (eco)hydrological studies. In addition to the frequent C-band Synthetic Aperture Radar (SAR) observations from Sentinel-1 (Torres et al., 2012) and the RADARSAT Constellation Mission (Thompson, 2015), other frequencies such as the L- and S-band mission NISAR (launch planned in 2023), the L-band mission ROSE-L (2028), and the P-band mission BIOMASS (2023) will

be available within the next decade (Rosen et al., 2017; Pierdicca et al., 2019; Quegan et al., 2019). Moreover, commercial providers such as Capella Space and ICEYE are building satellite constellations with X-band instruments (Farquharson et al., 2021; Ignatenko et al., 2020). These constellations will ensure multiple observations per day. As a result, the availability of spaceborne backscatter observations in the near future will offer a unique possibility to study vegetation water dynamics on different spatiotemporal scales.

However, we currently lack crucial knowledge on backscatter sensitivity to vegetation water dynamics. Soil moisture retrieval algorithms, for example, generally consider the confounding effects of vegetation water as time invariant or seasonally variant only (Kim et al., 2017). Well-established electromagnetic models have been developed and calibrated based on seasonally variant VWC only (e.g. Bracaglia et al., 1995). Moreover, the effect of surface canopy water (SCW), i.e. dew or rainfall interception, is also usually ignored (Vermunt et al., 2020; Xu et al., 2021). The omission of sub-daily vegetation water dynamics causes potential retrieval errors (Brancato et al., 2017) and, more importantly, hinders our understanding of the extent to which radar backscatter could be used to monitor vegetation water dynamics. Without this knowledge, the upcoming spaceborne observations cannot be used to their full potential.

Several studies have related observed diurnal backscatter cycles to vegetation water dynamics. Clear diurnal cycles were found in tower-based observations from forest stands (e.g. Hamadi et al., 2014; Monteith and Ulander, 2021) and agricultural cropland (e.g. Vermunt et al., 2020), as well as in aggregated satellite observations from larger forested areas (Paget et al., 2016; Emmerik et al., 2017; Konings et al., 2017). These studies have made important contributions to the understanding of sub-daily backscatter behaviour. However, a persistent challenge is the lack of in situ data for ground truth validation. In situ soil moisture can be routinely measured using a variety of sensors (Dobriyal et al., 2012; Cosh et al., 2016). Surface canopy water can be measured continuously using leaf wetness sensors (Cosh et al., 2009; Vermunt et al., 2020). However, internal VWC is still generally measured using laborious destructive sampling, particularly in agricultural fields (e.g. Vreugdenhil et al., 2018; Emmerik et al., 2015; Ye et al., 2021). This is acceptable for monitoring seasonal changes, but is prohibitively time-consuming and labour-intensive for sub-daily variations. Hence, it is crucial to find a more efficient way to obtain continuous, quantitative estimates of sub-daily VWC variations.

For woody constituents in trees, dendrometers have been used to infer water content non-destructively after detrending, and similarly, time- and frequency-domain reflectometry (TDR and FDR) and capacitance-style sensors have been used to derive water content indirectly by measuring dielectric permittivity (Konings et al., 2021). Moreover, a water balance-style approach using sap flow sensors have been

used by the tree physiology community to estimate diurnal changes in tree stem water storage (Goldstein et al., 1998; Meinzer et al., 2004; Čermák et al., 2007; Phillips et al., 2008; Köcher et al., 2013).

The objectives of this study were to test the potential of this non-destructive sap flow approach for estimating sub-daily VWC variations in herbaceous plants and to use these estimates to better understand what controls sub-daily variations in L-band backscatter. Specifically, we adapted this sap flow methodology, described in Sect. 2, to estimate 15 min changes in corn VWC using sap flow sensors and a weather station. An extensive data set from a field campaign in the Netherlands in 2019 was used to evaluate the adapted method against diurnal cycles of VWC obtained by destructive sampling. Finally, the technique was applied to reconstruct sub-daily VWC variability of multiple consecutive days from another field campaign in Florida in 2018. In this campaign, high temporal resolution tower-based polarimetric L-band backscatter was collected. The reconstructed VWC was used, together with simultaneously collected soil moisture and surface canopy water (SCW), to gain a better understanding of what controls sub-daily backscatter behaviour.

## 2 Estimating diurnal variations in tree water content using sap flow probes

Diurnal variations in internal VWC have been estimated in trees before, mainly in studies focused on understanding the functional role of stem water reserves on daily tree water use. A well-established in situ method uses sap flow probes at the base of the stem and in the crown (e.g. Goldstein et al., 1998; Meinzer et al., 2004; Čermák et al., 2007; Phillips et al., 2008; Köcher et al., 2013). This method is based on the time lag between transpiration and basal sap flow, as a result of a tree's hydraulic capacitance, which is the change in water content per unit change in water potential (e.g.  $\text{kg MPa}^{-1}$ ; Goldstein et al., 1998; Oguntunde et al., 2004). Morning transpiration, driven by the atmospheric evaporative demand, causes the depletion of internal VWC in the crown and, depending on the hydraulic capacitance, a drop in water potential. In response to the resulting potential gradient, sap flow rates increase to replenish the depleted VWC. As long as transpiration rates exceed basal sap flow rates, water is withdrawn from internal VWC, and when basal sap flow exceeds transpiration, internal VWC is refilled. Consequently, the diurnal variation in tree VWC could be calculated from the cumulative differences between basal sap flow and whole-crown transpiration (see the second term of Eq. 1).

$$\text{VWC}(t) = \text{VWC}(t_0) + \sum_{i=t_0}^t (F_i - T_i) \Delta t, \quad (1)$$

where  $\text{VWC}(t)$  is the estimated VWC at time  $t$ ,  $\text{VWC}(t_0)$  is a reference VWC at  $t = 0$ ,  $F$  is basal sap flow,  $T$  is whole-

crown transpiration, both in mass per unit of time, and  $\Delta t$  is the duration of a time step.

In these studies on trees, whole-crown transpiration was estimated from branch and basal sap flow based on two assumptions. First, time lags between branch sap flow in the crown and transpiration were assumed to be negligible compared to time lags between branch and basal sap flow. Hence, the averaged daily cycles of sap flow in the monitored branches were assumed to approximate the cycles of whole-crown transpiration. Second, most studies assumed that the 24 h sums of whole-crown transpiration and basal sap flow were equal (Goldstein et al., 1998; Čermák et al., 2007; Phillips et al., 2008; Köcher et al., 2013). This assumption made it possible to estimate whole-crown transpiration rates by first dividing averaged branch sap flow by its daily sum and then multiplying by the daily sum of basal sap flow. The corresponding assumption is that all water that is withdrawn from internal VWC is replaced within 24 h.

### 3 Data and methods

Section 3.1 relates to the adjustments and data required to make the sap flow approach (Sect. 2) applicable to corn. Data from a field campaign in the Netherlands in 2019 were used to evaluate the adjusted method. Section 3.2 relates to the methodology and data used from our field campaign in Florida in 2018 for interpreting sub-daily backscatter behaviour.

#### 3.1 Applying the sap flow approach to estimate diurnal variations in corn VWC

##### 3.1.1 Adjustments and evaluation of the sap flow approach

We investigated the potential of the sap flow method (Sect. 2) for estimating diurnal VWC variations in corn plants. The largest differences between corn plants and trees are related to hydraulic capacitance and structure. Corn plants have much lower hydraulic capacitance than most trees (Langensiepen et al., 2009) and, hence, shorter time lags between transpiration and basal sap flow. As a consequence, installing a sap flow sensor as a surrogate for transpiration would be problematic, since the assumption of a negligible time lag between transpiration and upper sap flow, compared to the lag with basal sap flow, is invalid. Moreover, transpiring corn leaves are somehow evenly distributed across the stem, in contrast to trees with a crown, which makes the placement of a second sensor to represent transpiration nearly impossible. For these reasons, we estimated transpiration using indirect estimates of reference evapotranspiration ( $ET_0$ ) instead. Details from sap flow measurements and  $ET_0$  estimates are given in Sect. 3.1.2.

A widely used approach to derive transpiration from  $ET_0$  is a linear conversion using crop factors, e.g. the FAO 56

dual-crop coefficient model (Allen et al., 1998). However, in many cases, these estimations systematically over- or underestimate direct observations of transpiration (Ding et al., 2013; Rafi et al., 2019) or sap flow (Langensiepen et al., 2009), while basal sap flow and transpiration at the leaves must equal over a sufficiently long time period (Swanson, 1994). For our data sets, Penman–Monteith-derived transpiration (Allen et al., 1998) is systematically lower than measured sap flow. Because sap flow is our most direct measurement, we chose to estimate transpiration by rescaling  $ET_0$  estimates using sap flow measurements. This means that information on the diurnal shape of  $ET_0$  is derived from the Penman–Monteith equation and that these  $ET_0$  estimates are then scaled so that the resulting transpiration estimates are consistent with sap flow over a given period of time.

We tested three different approaches to rescale  $ET_0$  estimates using sap flow measurements. The first approach was similar to the rescaling of branch sap flow to whole-crown transpiration in trees, described in Sect. 2. Transpiration was assumed to equal basal sap flow during a 24 h period, and 15 min  $ET_0$  estimates were divided by their 24 h sum and then multiplied by the 24 h sum of basal sap flow (see Eq. 2 in Table 1).

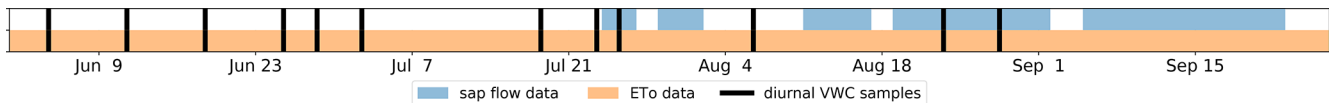
However, the assumption of complete replacement of withdrawn water within 24 h may not always hold. This is, for example, the case when water accumulates as a result of growth or when a plant is unable to replace the transpired water within a day as a result of stress. Therefore, we also tested the effect of either relaxing this assumption or using multiple days instead, i.e. 3, 5, or 7 consecutive days surrounding the day of interest or all measured days in the data set. Both approaches assume a simple, linear relation between  $ET_0$  and transpiration. It will be shown that this assumption can cause an offset between the timing of the diurnal cycles of sampled and reconstructed VWC. This issue was addressed by adopting the cumulative distribution function (CDF) matching method, previously used to rescale satellite-derived surface soil moisture to observations (Reichle and Koster, 2004; Drusch et al., 2005; Brocca et al., 2011). This nonlinear approach removes systematic differences between two data sets by matching the CDFs of both data sets (Brocca et al., 2011). Here, we matched the CDFs of the  $ET_0$  and sap flow data. This was achieved by first ranking all 15 min data from both data sets from low to high values and then fitting a second-order polynomial function through the scatterplot of both ranked data sets. Subsequently, this function was used to convert the 15 min  $ET_0$  data to transpiration estimates. CDF matching was also performed for 1, 3, 5, and 7 consecutive days and all available days. Figure 4 illustrates CDF matching and its results for 3 d of our data.

VWC samples obtained by destructive sampling during the 2019 campaign (Sect. 3.1.2) were used to validate the method. For the selected days (Fig. 1), we used one of the five sampling times to constrain the daily cycle ( $VWC(t_0)$  in Eq. 1). The other four independent samples were com-

**Table 1.** The three tested approaches to estimate transpiration ( $T$ ) using Penman–Monteith-derived  $ET_0$  estimates and sap flow measurements.

Approach	Assumptions	Equations
Linear – 24 h	Withdrawn water is replaced within 24 h; $T$ is linearly related to $ET_0$	$T(t) = ET_0(t)F_{24h}/ET_{0_{24h}}$ (2)
Linear – multiple days	Withdrawn water is replaced within $n$ days; $T$ is linearly related to $ET_0$	$T(t) = ET_0(t)F_{nd}/ET_{0_{nd}}$ (3)
Nonlinear – CDF matching	Withdrawn water is replaced within $n$ days; CDF of $T$ equals CDF of $F$	$T(t) = a^{**}ET_0(t) + b^{**}ET_0(t)^2$ (4)

\* Subscripts 24 h and  $nd$  relate to the 24 h sum and  $n$  number of days sum, respectively. \*\*  $a$  and  $b$  are found by a second-order polynomial fit through ranked  $F$  and  $ET_0$  data, as illustrated in Fig. 4c.

**Figure 1.** Availability of the data required to evaluate the adjusted methodology for estimating 15 min VWC variations. The availability of the sap flow,  $ET_0$ , and sampling data matched on 25 July and 23 and 28 August.

pared against the estimated diurnal cycle of VWC variations. For each day, we calculated the root mean square error (RMSE) between the four independent samples and reconstructed VWC on these four times. All five samples were used as ( $VWC(t_0)$ ) once to determine the best time to constrain the reconstruction.

In summary, we adapted and evaluated the sap flow methodology to estimate diurnal cycles of corn VWC through the following three steps.

1. The diurnal cycle of transpiration was estimated from  $ET_0$  and sap flow data, using three different approaches (Table 1).
2. Sub-daily variations in VWC were estimated by calculating the cumulative difference between 15 min basal sap flow and transpiration estimates (Eq. 1).
3. The resulting estimates of diurnal VWC variations were compared against destructive measurements of VWC.

### 3.1.2 Experimental site and data collection

#### Experimental site 2019

The field campaign in The Netherlands was conducted in Reusel (51.319° N, 5.173° E), at Van Den Borne Aardappelen. There, field corn was planted on a sandy soil with a density of eight plants per square metre (hereafter  $m^{-2}$ ), and harvested, for silage after the required senescence, 148 d after planting. The Netherlands has a temperate maritime climate. However, maximum national temperature records were broken close to the field site during the growing season of 2019, and it was the second anomalously dry summer in a row (Bartholomeus et al., 2020).

#### Sap flow

Sap flow was monitored near the base of the stem using stem flow gauges produced by Dynamax Inc. (Houston, TX, USA). The measurement is based on the stem heat balance theory (Sakuratani, 1981). A flexible collar strap with built-in heater strip and thermocouples is wrapped around a corn stem, about 20 cm above the ground, and is then isolated and protected from environmental conditions such as rain and radiation. The entire circumference of the stem receives a constant heat input from the heater strip. As sap movement carries heat, thermal dissipation corresponds to the sap flow rate. Therefore, the change in temperature is used as a tracer for sap flow ( $g\ h^{-1}$ ), thereby taking into account the heat transfer to the stem tissue and the ambient air. Conversion to millimetres per 15 min ( $mm\ 15\ min^{-1}$ ) was performed using the density of liquid water and the planting density. Because the collar straps are designed to fit a certain range of stem diameters, we collected data in the mid- and late season.

In 2019, a maximum of two sensors were installed due to power limitations. Because one sensor failed, the used data are from a single sensor. Gaps in the time series were caused by disturbances in the connection with the battery.

#### Reference evapotranspiration

A weather station was installed at the edge of the experimental site, with a ECH2O rain model ECRN-100 rain gauge, Apogee SP-212 pyranometer (solar radiation), a Davis Cup anemometer (wind and gust speed and wind direction), and a HOBO Temperature/RH Smart Sensor model S-THB-M008 (temperature and relative humidity). Reference evapotranspi-

ration ( $ET_0$ ) was estimated using the Penman–Monteith approach described by Zotarelli et al. (2010).

### Sampling

Vegetation water content (VWC) was measured by destructive sampling. For each sampling time, six field-representative samples were taken from designated sampling areas. Any present dew or interception was removed with paper towels before the samples were weighted to determine the average fresh biomass per plant in kilograms ( $m_f$ ). Samples were oven-dried at 60°C for 4–8 d, depending on the growth stage. These dried samples were weighed again to determine average dry biomass per plant in kilograms ( $m_d$ ). Field-representative VWC ( $\text{kg m}^{-2}$ ) was estimated by multiplying the evaporated water per plant (kg) with the number of plants per  $\text{m}^2$  ( $\rho_{\text{plant}}$ ; see Eq. 5).

$$\text{VWC} = (m_f - m_d) \rho_{\text{plant}}. \quad (5)$$

In 2019, we aimed to capture full diurnal cycles of VWC. Hence, we sampled at five equally distributed times, between sunrise and sunset, on 12 d spread throughout the season. Seasonal VWC variations were monitored by predawn sampling only.

Figure 1 shows the availability of the data required to evaluate the adjusted methodology for estimating 15 min VWC variations. The availability of sap flow,  $ET_0$ , and VWC sampling data matched on 25 July and 23 and 28 August.

### Surface canopy water and soil moisture

Measurements of surface canopy water (dew and interception) and root zone soil moisture were used as ancillary data sets to support the evaluation of the reconstructed VWC estimations. Surface canopy water (SCW) was monitored using PHYTOS 31 leaf dielectric wetness sensors. A total of three sensors were installed on different heights in the vegetation layer, and one sensor failed during the season. Measured leaf areas were used to convert sensor output to full-canopy SCW ( $\text{kg m}^{-2}$ ). Details of this conversion and sensor properties are described in Vermunt et al. (2020).

Soil moisture ( $\theta$ ) was observed in two pits with 15 min resolution, using EC-5 sensors at 5, 10, 20, 40, and 80 cm depth. These measurements were averaged based on depth. Root zone soil moisture was estimated by integrating the measurements from all depth over a soil column of 100 cm, based on the thickness of the soil layer associated with the depth of the sensor.

## 3.2 Interpreting the behaviour of sub-daily L-band backscatter

### 3.2.1 Approach and data requirement

To gain a better understanding of what controls sub-daily L-band backscatter behaviour, we analysed tower-based obser-

vations using continuous time series of the three moisture stores in the corn field, namely (1) VWC, (2) SCW, and (3) surface soil moisture ( $\theta$ ). Details of the collection of these time series are given in Sect. 3.2.2. The longest period for which we had all data available was from 4 June 00:00 LT to 13 June 10:15 LT. During this period, the corn is at maximum height and leaf area index (LAI) and is 1–2 weeks before harvest on 18 June. All analyses were conducted for this period.

Insights in the separate effects of the three different moisture stores on sub-daily backscatter ( $\sigma^0$ ) variations were gained by quantifying their relations through multiple linear regression. The relation between sub-daily backscatter variations and changes in these dynamic moisture stores was described as follows:

$$\begin{aligned} \sigma^0(t) = & \sigma_{t_0}^0 + a(\theta_t - \theta_{t_0}) + b(\text{VWC}_t - \text{VWC}_{t_0}) \\ & + c(\text{SCW}_t - \text{SCW}_{t_0}), \end{aligned} \quad (6)$$

where  $t_0$  is the first radar acquisition time of the day (01:00 LT) and assumes linear relations between  $\sigma^0$  and the individual moisture stores. The regression coefficients  $a$  ( $\text{dB m}^{-3} \text{m}^{-3}$ ),  $b$  ( $\text{dB kg}^{-1} \text{m}^{-2}$ ), and  $c$  ( $\text{dB kg}^{-1} \text{m}^{-2}$ ) were used to quantify the change in backscatter within a day as a result of change in moisture and were derived for each polarization separately.

### 3.2.2 Experimental site and data collection

#### Experimental site 2018

The field campaign in Florida, USA, was conducted in Citra (29.410° N, 82.179° W), at the Plant Science Research and Education Unit (PSREU) of the University of Florida and the Institute of Food and Agricultural Sciences (UF/IFAS). Sweetcorn was planted in a sandy soil, with a density of 7.9 plants per  $\text{m}^{-2}$ , and harvested after 66 d, in mid-June, for human consumption. The climate of this area in Florida is humid subtropical, and the 2018 spring growing season was characterized by high temperatures, high-intensity rainfall, and thunderstorms.

#### Backscatter

High temporal resolution L-band backscatter data were collected with the polarimetric University of Florida L-band Automated Radar System (UF-LARS) throughout the growing season of 2018. This system was mounted on a Genie aerial work platform at a height of 14 m above the ground. The scatterometer scanned the cornfield, with an incidence angle of 40°, and acquired 16 observations spread throughout the day in the late season. The installation of sensors and vegetation sampling was performed outside the arc swept by the radar. A comprehensive description of the observations and the UF-LARS system can be found in Vermunt et al. (2020) and Nagarajan et al. (2014), respectively. Cross-polarization (cross-pol) is used to refer to the average of the HV- (horizon-

tal transmit and vertical receive) and VH-polarized (vertical transmit and horizontal receive) backscatter.

### Reconstruction of diurnal VWC variations for multiple consecutive days

To support the analysis of variations in the L-band backscatter, a 10 d time series of diurnal VWC variations was reconstructed for the 2018 data. The methodology used for the reconstruction was based on adjustments and evaluation of the sap flow approach presented in Sect. 3.1.1. The required sap flow and  $ET_0$  data sets were similar but slightly different. In 2018, four sap flow sensors were installed simultaneously on four different plants, and the data were averaged. Gaps in the time series were caused by disturbances in the connection with the battery or solar panel.

Meteorological data with 15 min resolution were obtained from the nearby Florida Automated Weather Network (FAWN) weather station, located within 600 m from the experimental field. Observations of rainfall, air temperature (2 m), solar radiation, relative humidity, and wind speed were downloaded from the Report Generator (<https://fawn.ifas.ufl.edu/data/reports/>, last access: 10 October 2018).  $ET_0$  was estimated using the same Penman–Monteith approach described by Zotarelli et al. (2010).

In contrast to the 2019 data set, VWC samples were not collected to capture the full diurnal cycle. Instead, these samples were obtained 4 times per week, i.e. 3 d at 06:00 LT, and also at 18:00 LT on one of these days, originally to capture differences between morning and evening passes for a sun-synchronous satellite such as SMAP (Soil Moisture Active Passive; Entekhabi et al., 2010). Moreover, the presented VWC data for 2018 are averages of eight plants instead of six. The samples were used to constrain the reconstructed VWC variations.

The period of consecutive days for the analysis was limited by the availability of sap flow data. A 10 d time series was found in mid- to late season which contained continuous sap flow and weather data, L-band backscatter, and 5 sampling days. On these days, samples were used to constrain the VWC record. On the 5 d without sampling, the VWC records were constrained either at the end of previous sampling day (forward reconstruction) or at the start of next sampling day (backward). In case there was a gap between the forward and backward reconstructions, the average of both was considered the best estimate of VWC.

### Soil moisture and surface canopy water

For the analysis of sub-daily variations in the L-band backscatter, we also collected 15 min variations in surface soil moisture, at 5 cm depth, and SCW. Together with VWC, they form the moisture stores of a cornfield which are considered to affect sub-daily backscatter. Details of the sensors and

measurements are described in Sect. 3.1.2 and extensively in Vermunt et al. (2020).

## 4 Results

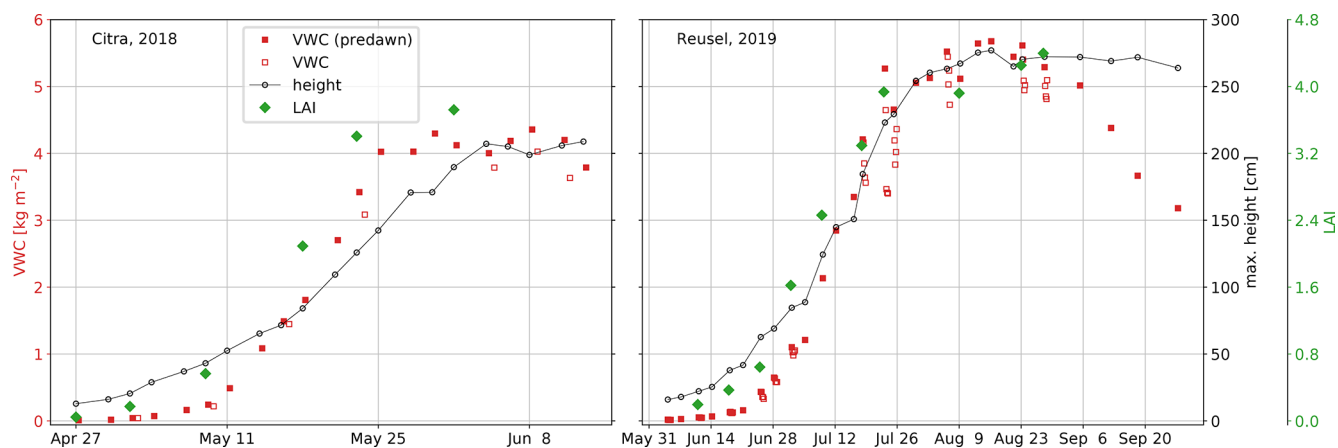
### 4.1 Seasonal and diurnal variation of vegetation water content

Figure 2 illustrates the seasonal and diurnal variations of VWC ( $\text{kg m}^{-2}$ ) from destructive sampling in the 2018 and 2019 campaigns. From the early to mid-season, VWC increased as a result of biomass accumulation. The field corn from 2019 was allowed to senesce before harvest, resulting in a significant reduction in water storage in the plants from 23 August onward. The sweetcorn from 2018 was harvested before considerable senescence.

The open markers are the non-predawn measurements, which were at 18:00 LT (2018), and at four evenly distributed times between sunrise and sunset (2019). The range of these latter diurnal measurements gives an indication of the amplitude of the daily cycle of VWC. On most days, the diurnal minimum was 10 %–20 % lower than the predawn water storage. An exception was 23 July, when predawn water storage was depleted by 35.4 % during the day. Figure 3 magnifies the mid-season measurements and illustrates the difference between water depletion in the non-stressed conditions compared to the stressed date. The photograph was taken around the third measurement on 23 July. This picture shows leaf rolling, which is a mechanism to reduce the leaf area exposed for transpiration and a sign of drought stress. Normal-shaped leaves were observed again as a result of irrigation, which was applied right after the last sampling on 23 July, in order to ensure the crop's survival.

### 4.2 Reconstructions of continuous, sub-daily variations in vegetation water content

As described in Sect. 3.1.1, we tested three approaches to estimate transpiration from  $ET_0$  and sap flow. As an alternative to the straightforward linear conversions, we proposed to test the nonlinear CDF matching principle (Table 1). Figure 4 illustrates the procedure of estimating transpiration using this principle, using 3 d of sap flow and  $ET_0$  data. We take 25 July 2019 as an example and use the data from 24 and 26 July as well (Fig. 4a). On 25 July, which was particularly warm and sunny, we measured a maximum temperature of 39.0 °C in the field. Figure 4b illustrates the difference between the CDFs of sap flow and  $ET_0$ , which is particularly evident at the 35 % highest rates. At lower rates ( $< 0.07 \text{ mm } 15 \text{ min}^{-1}$ ),  $ET_0$  rates were slightly higher than sap flow rates. As these systematic differences between both rates may be unrealistic, a second-order polynomial was fitted through the scatterplot with ranked  $ET_0$  and sap flow data (Fig. 4c) and was used to match the CDFs (Fig. 4d). The resulting CDF-matched transpiration estimate (T-cdf; Fig. 4e)



**Figure 2.** Vegetation water content (VWC), crop height, and leaf area index (LAI) from the field experiments in Citra (2018) and Reusel (2019). Filled red markers indicate predawn measurements, while open markers indicate non-predawn measurements at 18:00 LT (2018) and morning to sunset (2019).

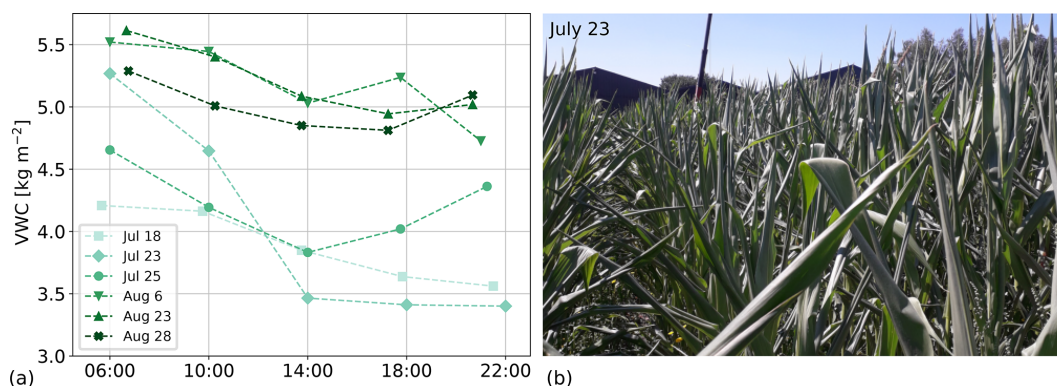


**Figure 3.** Sampled vegetation water content (VWC) in the mid-season, 2019 (a), and a picture of rolled leaves (b), taken around the third measurement on 23 July, as a sign of drought stress.

was used to estimate  $\Delta\text{VWC}$  at any point in time using the approach described in Fig. 5.

The procedure to reconstruct 15 min changes in VWC is depicted in Fig. 5, again with 25 July as an example. Figure 5a illustrates the effects of the three approaches on estimate transpiration from  $\text{ET}_0$  and sap flow (Table 1). T-cdf and T-3 d represent the CDF-matched and linear estimates of transpiration, for which 3 d of data were used, i.e. 24–26 July. What stands out is that the CDF-matched rescaling (T-cdf) provides a significantly higher peak compared to the linear rescaling (T-24 h and T-3 d). On the other hand, when  $\text{ET}_0$  rates are  $0.09 \text{ mm } 15 \text{ min}^{-1}$  or lower, T-cdf was lower than the linear estimates. Both linear transpiration estimates were close in this particular case, which means that the ratio of the 24 h sum of sap flow over  $\text{ET}_0$  was close to the ratio of the 3 d sum of sap flow over  $\text{ET}_0$ . Figure 5b shows the diurnal cycles of basal sap flow ( $F$ ) and transpiration. Here, the simplest linear transpiration estimate (T-24 h) was depicted as an example. The difference between sap flow and transpiration gave the estimated depletion and refilling of internal

water storage (Fig. 5c). If transpiration rates exceeded sap flow rates at some point in time, the line is below zero, which indicates a depletion of water storage. Positive values indicate refilling. Finally, the cumulative difference between sap flow and transpiration represents the diurnal change in plant water storage or  $\Delta\text{VWC}$  (Fig. 5d). The minimum VWC was reached around 12:45 LT, when  $0.87 \text{ kg m}^{-2}$  of the predawn water storage was depleted. This is close to the maximum diurnal difference of  $0.82 \text{ kg m}^{-2}$  observed on that day from destructive sampling (Fig. 3).

Diurnal cycles of VWC were reconstructed for both linear and nonlinear transpiration estimates, using  $\Delta\text{VWC}$  (Fig. 5d) and one destructive sample (Figs. 2 and 3) per day as a constraint. Results were compared against the other destructive samples. The effect of both the time of the constraint and the number of days considered for the transpiration estimation on the VWC reconstructions were evaluated. The RMSEs of the 2019 data are presented in Tables A1–A2. A general optimal combination of the time of the constraint and the number of days to consider could not be found. Using CDF-matched



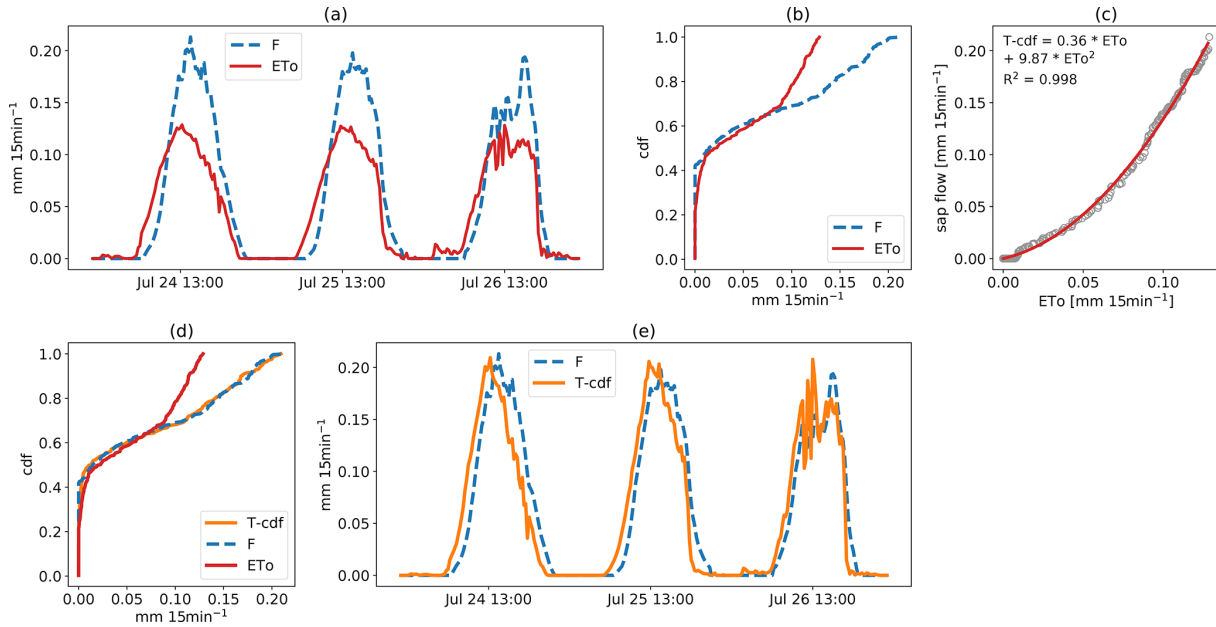


**Figure 4.** Example of  $ET_0$  rescaling to approximate transpiration (2019 campaign), using the CDF matching approach. **(a)** Sap flow ( $F$ ) and reference evapotranspiration ( $ET_0$ ) data from 24–26 July 2019. **(b)** Cumulative distribution function (CDF) of both data sets in this period. **(c)** Second-order polynomial fit through ranked  $F$  and  $ET_0$  data, used to derive the CDF-matched transpiration estimate (T-cdf), which was added to the CDF plot in panel **(d)**. Panel **(e)** shows the final result of the CDF matching.

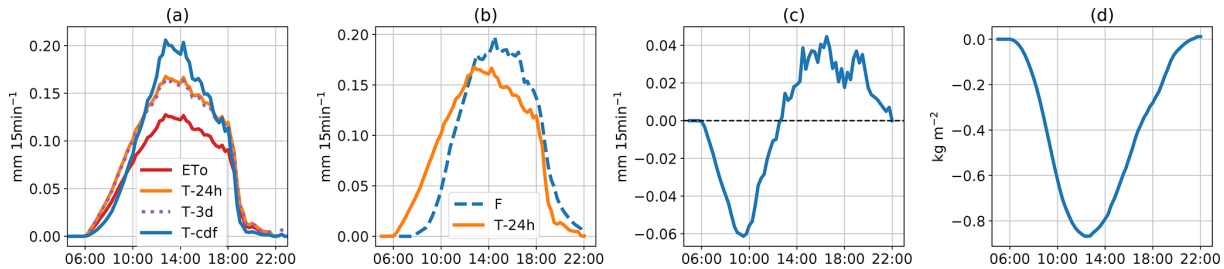


**Figure 5.** A four-step procedure to reconstruct the diurnal variation in VWC. An example for 25 July 2019. Panel **(a)** shows the diurnal cycles of reference evapotranspiration ( $ET_0$ ) and the three transpiration estimates (see Table 1). Panel **(b)** shows the diurnal cycles of sap flow ( $F$ ) and one of the transpiration estimates (T-24 h). Panel **(c)** is the difference between sap flow and transpiration, where negative values indicate depletion of water storage, and positive values indicate refill. Panel **(d)** illustrates the resulting cumulative change in stored water ( $\Delta VWC$ ) during the day.

transpiration estimates resulted in a better agreement with the destructive sampling data than using linear correction in 80 % of the cases. The best reconstructions from 2019 (Tables A1 and A2) are presented in Fig. 6 and differentiated by the approach to estimate transpiration. Differences between environmental conditions are shown in Fig. 7. Figure 6 illustrates the improvement of the reconstruction when using more than 1 d of data for the estimation of transpiration (second and third rows). The upper row clearly shows that the linear 24 h approach does not allow for a difference between the start- and end-of-day VWC, while the inclusion of multiple days does. Besides, the reconstruction on 25 July illustrates the possible improvement that CDF matching can have. On 25 July and 28 August, the RMSEs of the lowest plots were

8 % and 12 % of the amplitude of the diurnal cycles, respectively. On 23 August, the agreement is poor, especially later in the day, and this percentage is 36.9 %. On this day, reconstructions and samples disagree for all three approaches to estimating transpiration but less so for the CDF matching procedure.

For the 2018 campaign, we had a maximum of two VWC samples per day. Table A3 shows the offset between one of the samples and the reconstructed VWC, which was constrained by the other sample for 4, 8, and 11 June. The lowest offsets were found when transpiration was estimated using all data (12 d), and when CDF matching was applied. Consequently, we used the transpiration calculated based on this combination for further use of reconstructed VWC.

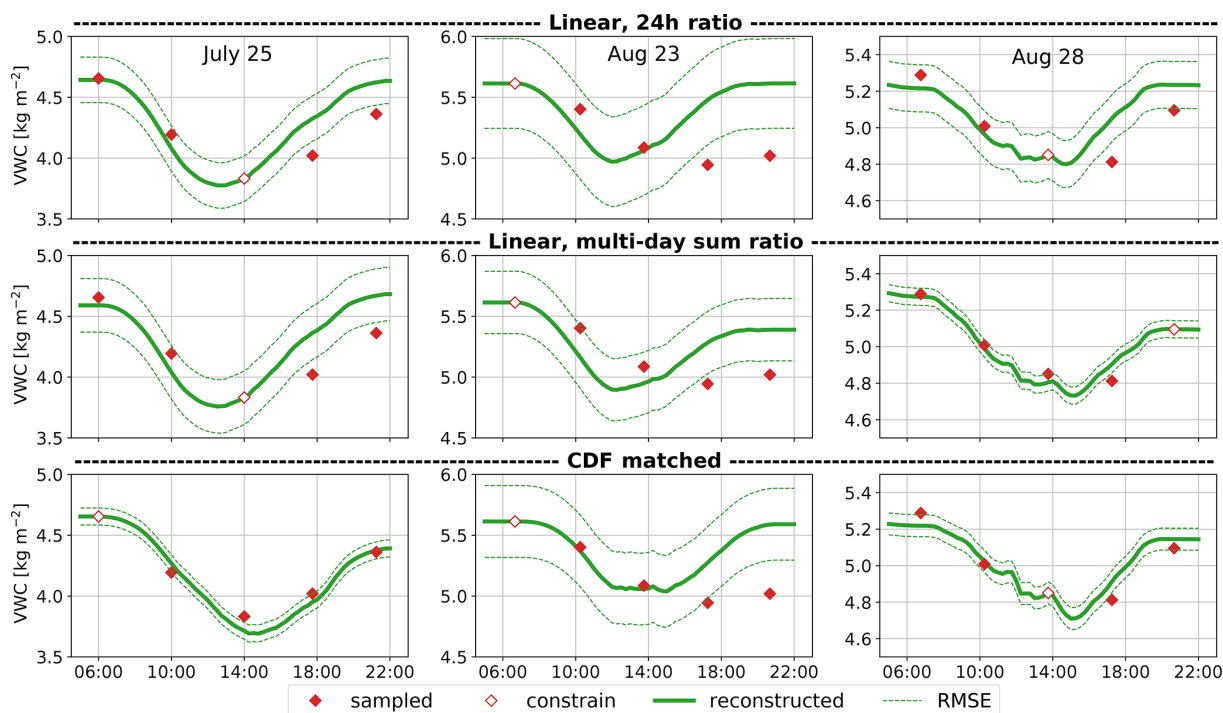


**Figure 6.** Best diurnal VWC reconstructions for 25 July and 23 and August 28 (2019) for three different methods of estimating transpiration. The upper row shows the results for using the simplest, linear estimate of transpiration. The middle row shows the reconstructions using linear estimates of transpiration but now considering 3, 5, and 7 d rather than 24 h. The lower row shows the results after CDF matching, considering all data, and 5 and 3 d for the CDF matching, respectively. The dashed green lines represent one RMSE above and one RMSE below the reconstructed VWC. The measurement which is used to constrain the reconstructed line is accentuated with an open marker.

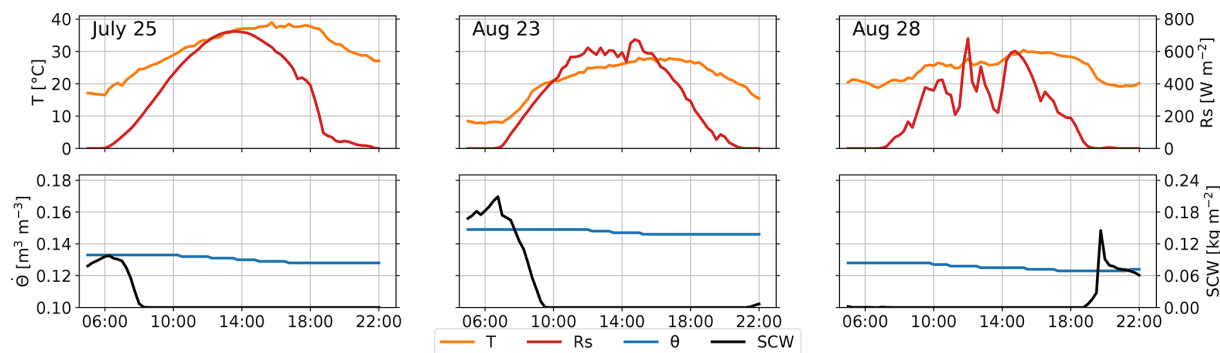


**Figure 7.** Environmental conditions on the sampling days of 25 July and 23 and 28 August (2019). The upper row shows air temperature ( $T$ ) and solar radiation ( $R_s$ ), and the lower row shows root zone soil moisture ( $\theta$ ) and surface canopy water (SCW).

### 4.3 Reconstructing a record of multiple days

Figure 8 shows the procedure for reconstructing the 10 d VWC record from 2018 data. On 4, 8, and 11 June, evening samples (18:00 LT) were used as constraints rather than predawn samples (06:00 LT), which resulted in smaller gaps between consecutive days (Fig. 8c). On days without sampling, VWC records were the averages of forward or backward reconstructions. On 9 and 10 June, the weighted aver-

age based on the distance to the sampling date was considered as the best estimate of VWC.

The diurnal VWC pattern on 5 and 6 June seems physically implausible because one would not expect an enormous increase in VWC on the warmest and driest day (5 June) and a drop on the most rainy/cloudy day (6 June). Despite the advantage of CDF matching, as opposed to linear conversion to better reflect diurnal extremes, the anomalous dynamics of 5 and 6 June are not captured sufficiently.

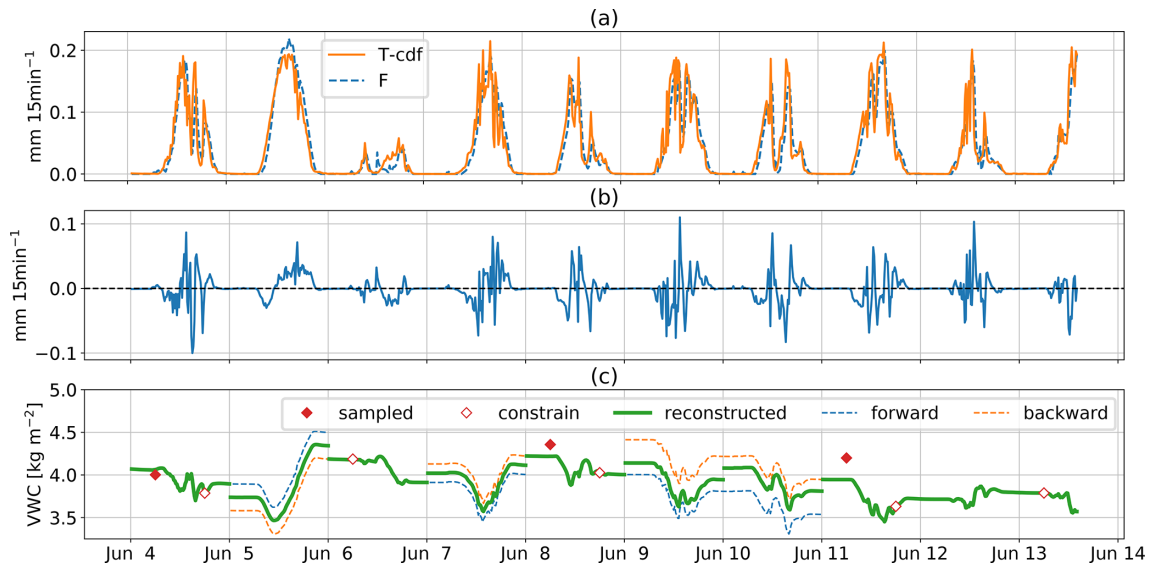


**Figure 8.** A 10 d reconstruction of VWC, with (a) sap flow ( $F$ ) and estimated transpiration ( $ET_0$ -cdf). (b) The difference between sap flow and transpiration and (c) the sampled and reconstructed VWC is shown. In between sampling days, VWC estimates are the weighted average between forward and backward reconstructions from the consecutive sampling days (based on the time to the closest sampling day). The measurements which are used to constrain the reconstructed line are accentuated with open markers.

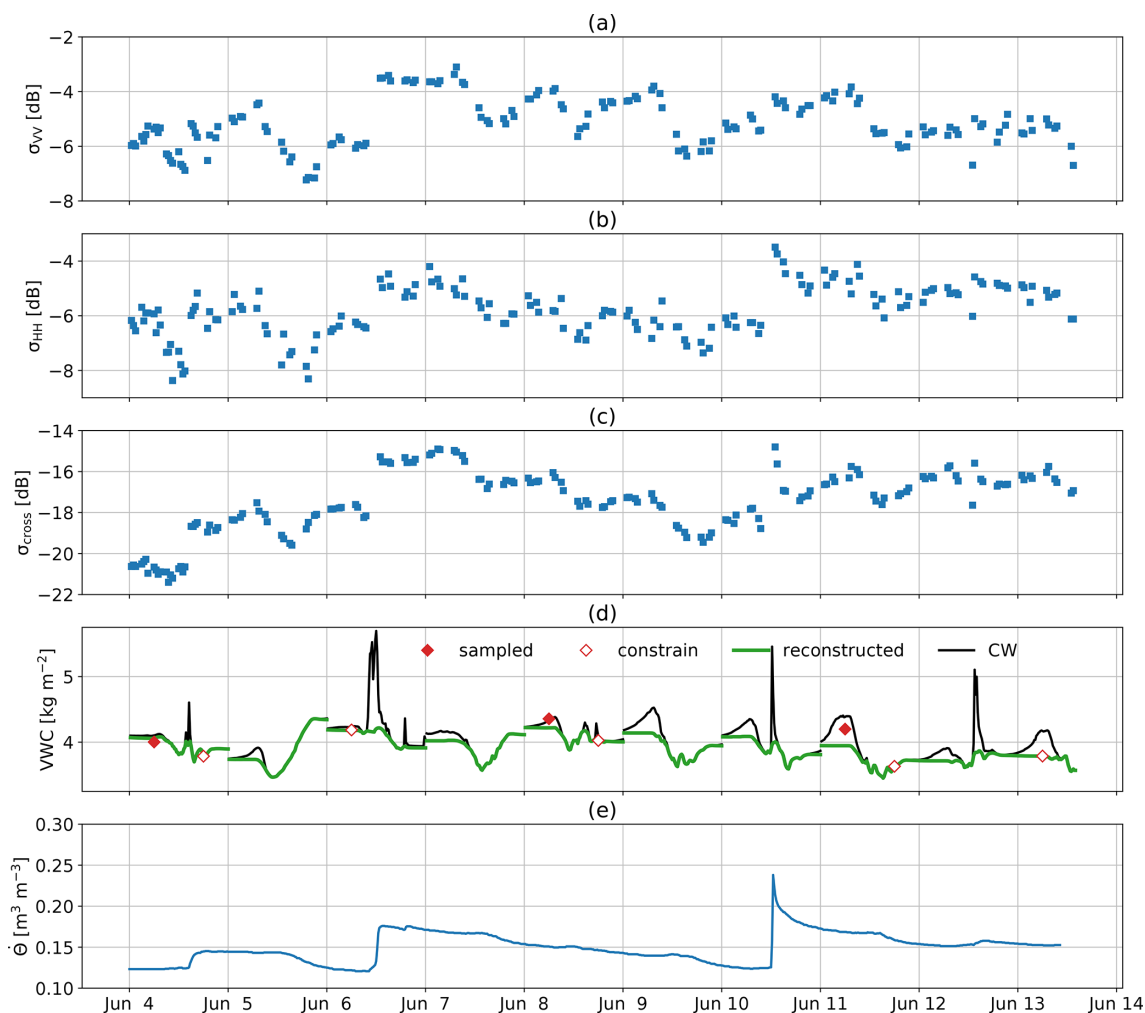
#### 4.4 The effect on sub-daily L-band backscatter

Figure 9 illustrates the potential value of reconstructing VWC records for interpreting the time series of microwave remote sensing data, in this case L-band backscatter. The upper three panels show the VV- (vertically), HH- (horizontally) and cross-polarized backscatter coefficients, respectively. Figure 9d shows the sampled and reconstructed VWC, together with the total canopy water (CW), which is the sum of the reconstructed VWC and SCW ( $\text{kg m}^{-2}$ ). The latter is either rainfall interception, which is characterized by rapid increases and is often transient because of daytime evaporation, or dew formation, which accumulates gradually during the night and dissipates quickly after sunrise. Figure 9e shows the volumetric soil moisture at  $-5$  cm depth.

Sub-daily variability of  $> 2$  dB was found in all three polarizations. A sharp backscatter increase after rainfall was observed in all polarizations. Slow downward trends were also found, corresponding with the drydown in soil moisture. However, on a sub-daily timescale, the backscatter variability shows strong similarities with diurnal patterns of canopy water (Fig. 9d). These diurnal cycles are most clearly visible in VV-pol. Figure 10 magnifies the diurnal variations for 3 d without rainfall, i.e. 7, 9, and 11 June. These days demonstrate clear similarities between the diurnal behaviour of the backscatter, mainly VV- and cross-pol, and canopy water. These similarities are particularly present in the period between midnight and mid-afternoon, when surface soil moisture is relatively stable. In fact, when randomly occurring rain events are excluded, the sub-daily backscatter behaviour can be analysed using the following three distinct sub-daily

periods: (1) from midnight to early morning, (2) from early morning to afternoon, and (3) from afternoon to midnight. The aggregated data in Fig. 11 help to visualize the dynamics in these periods. Because rain fell more often in the afternoon and evening, the exclusion of periods with rainfall led to data aggregation across 9, 6, and 4 d in these three periods, respectively. Around midnight, dew started to form until its peak between 07:00 and 07:30 LT, which is within 1 h after sunrise around 06:30 LT. In this same period, VWC was stable and surface soil moisture decreased slightly. VV- and cross-polarized backscatter increased, following dew formation, while HH-polarized stayed relatively stable. From early morning (07:30 LT) to afternoon (14:00 LT), dew dissipated and VWC dropped significantly. The same holds for backscatter in all polarizations, while surface soil moisture was still relatively stable. Finally, the last period of the day is characterized by the refilling of the plant's internal water storage and a decrease in soil moisture. The fact that backscatter in all polarizations remains relatively constant between 15:00 and 19:30 LT suggests the counterbalancing effects of soil moisture and VWC on backscatter in this period. During the last four aggregated acquisitions between 19:00 and 21:30 LT, VV- and cross-polarized backscatter show a slightly increasing trend similar to VWC.

The separate effects of the different moisture stores on backscatter ( $\sigma^0$ ) were quantified through multiple linear regression. Because we considered the VWC reconstructions from 5 and 6 June as being less reliable, the period between 7 and 13 June was used for the regression. Table 2 presents the estimated regression coefficients found for this period (see Eq. 6). A summary of the multiple linear regres-



**Figure 9.** Full polarimetric L-band backscatter and separated effects for a 10 d period near the end of the growing season in 2018, with (a) VV-polarized scattering coefficient, (b) HH-polarized scattering coefficient, and (c) averaged VH- and HV-polarized scattering coefficients, (d) sampled and reconstructed VWC, total canopy water, which is the sum of reconstructed VWC and SCW, and (e) soil moisture at 5 cm depth. The measurements which are used to constrain the reconstructed line are accentuated with open markers.

**Table 2.** Estimated regression coefficients per polarization for the period 7–13 June 2018 (Eq. 6).

	VV-pol	HH-pol	Cross-pol
$a$ (dB m <sup>3</sup> m <sup>-3</sup> )	24.06	39.47	38.83
$b$ (dB kg <sup>-1</sup> m <sup>-2</sup> )	2.93	2.29	2.45
$c$ (dB kg <sup>-1</sup> m <sup>-2</sup> )	0.62	0.38	0.73

sion statistics is given in Table A4 in the Appendix. The regression coefficients suggest that, from all polarizations, VV-pol was most sensitive to internal vegetation water storage and least sensitive to soil moisture. Compared to other polarizations, HH-pol was least sensitive to VWC and SCW and most sensitive to soil moisture. Cross-pol was more sensitive to SCW than the other polarizations. Note that the coeffi-

cients from soil and vegetation water stores (Table 2) have non-homogeneous physical units. Nonetheless, these coefficients indicate that, for a typical dry day during the campaign of 2018, e.g. 9 June, the soil moisture reduction of 0.015 m<sup>3</sup>m<sup>-3</sup> translates to a  $-0.4$ ,  $-0.6$ , and  $-0.6$  dB change in VV-, HH-, and cross-polarized backscatter, respectively. During the same day, VWC changed by 0.5 kg m<sup>-2</sup>, which would translate to a change of 1.5 dB (VV), 1.2 dB (HH) and 1.2 dB (cross). This indicates that, on this typical dry day, a diurnal variation in VWC leads to an almost 4 times higher change in VV-polarized backscatter (dB) than a diurnal change in soil moisture does. On the same day, the changes in HH- and cross-polarized backscatter (dB) were 2 times higher for the diurnal VWC variations than for the soil moisture drydown. The 0.4 kg m<sup>-2</sup> dew formation and dissipation caused  $\sigma^0$  to vary by 0.2 dB (VV), 0.2 dB (HH), and 0.3 dB (cross).

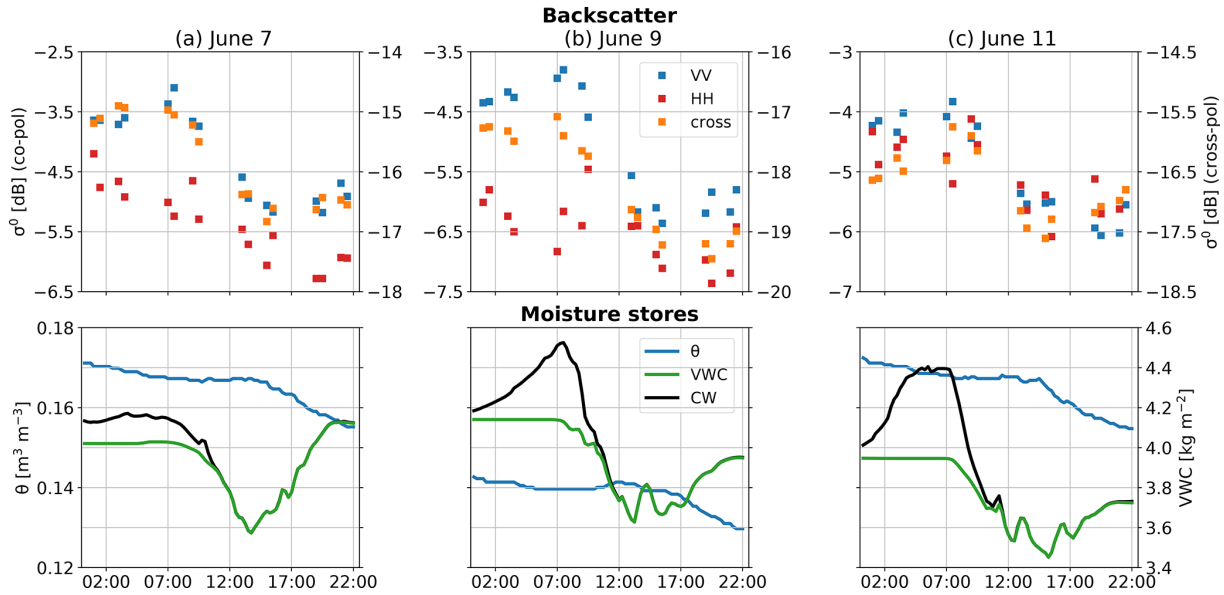


**Figure 10.** Diurnal behaviour of backscatter (VV-, HH-, and cross-pol) and moisture (soil moisture, VWC, and SCW) for 3 individual days without rainfall. These days were selected from the period presented in Fig. 9.

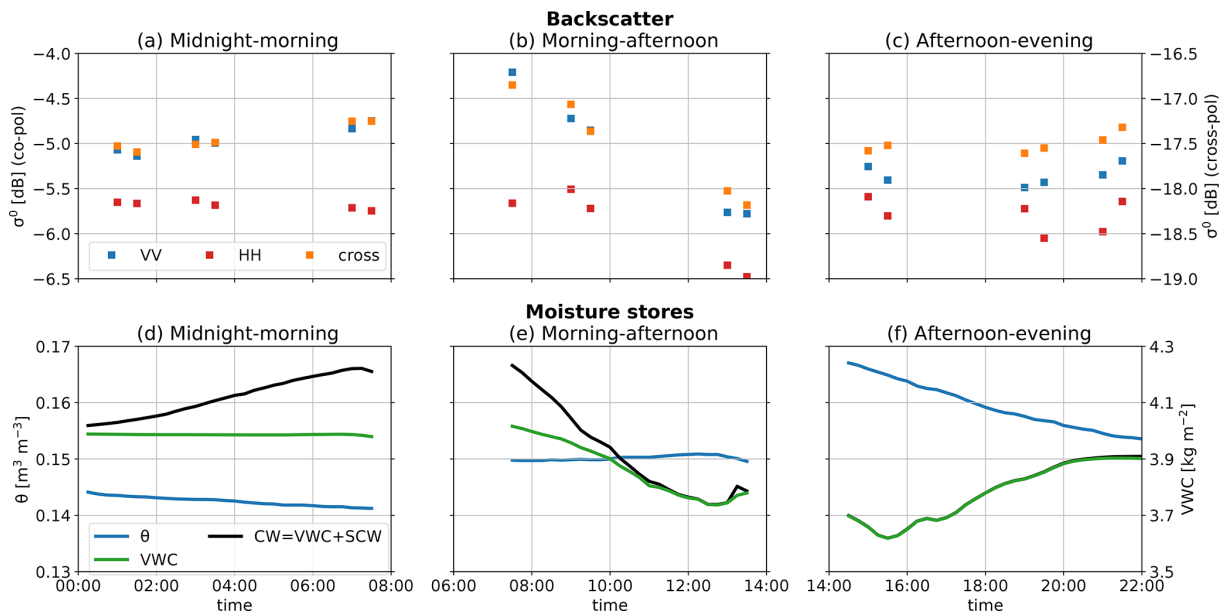


**Figure 11.** Backscatter (VV-, HH-, and cross-pol) and moisture (VWC, CW, and  $\theta$ ) data aggregated across multiple days and separated by part of the day, i.e. midnight–morning, morning–afternoon, and afternoon–midnight. Periods with disturbing rain events are excluded, which means that data in panels (a, d), (b, e), and (c, f) are aggregated across 9, 6, and 4 d, respectively. Canopy water (CW) is SCW displayed on top of VWC.

Figure 12 presents the results of using the regression coefficients (Table 2) and the time series of VWC, SCW, and soil moisture to describe diurnal variations in backscatter. Each day is constrained by the first radar observation of the day at 01:00 LT. Note, from the  $R^2$  values in Table A4, that 68%–71% of the variance in backscatter is explained by the three predictors. The  $P$  values for SCW are always higher than

those for VWC and soil moisture. Nonetheless, with the exception of the SCW coefficient in the case of HH backscatter ( $P > |t| = 0.286$ ), all  $P$  values are  $< 0.05$ , indicating statistical significance. However, note from Fig. 12a and c that the observed nocturnal backscatter increase as a result of dew formation is barely visible in the calculated backscatter. This

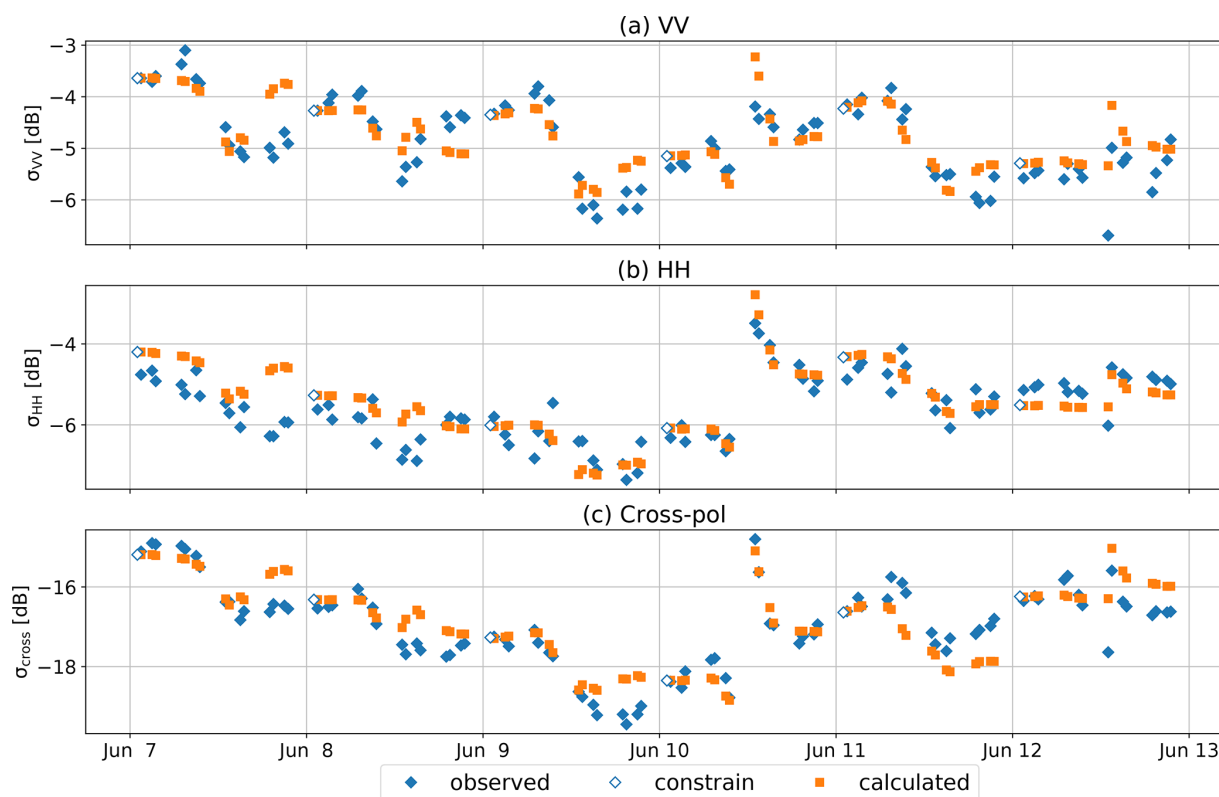


**Figure 12.** Observed and calculated (a) VV-, (b) HH-, and (c) cross-polarized  $\sigma^0$  from 7–13 June 2018. The observations which are used to constrain the predictions of sub-daily  $\sigma^0$  variability,  $\sigma_{t_0}^0$ , are accentuated with open markers. Sub-daily backscatter variation is calculated using Eq. (6), the coefficients found by multiple linear regression (Table 2), and the time series of VWC, SCW, and soil moisture.

suggests that the regression underestimates the effect of dew on backscatter.

## 5 Discussion

### 5.1 Sub-daily vegetation water content estimates: observations and reconstructions

Our results showed that, in non-stressed conditions, VWC depleted by 10%–20% during the day. This internal VWC withdrawal is approximately 10%–20% of the total daily transpiration, which is similar to findings from tropical and temperate broadleaved trees (Meinzer et al., 2004; Köcher et al., 2013). In stressed conditions, we found a 35% drop of VWC during the day.

We tested the potential of a non-destructive sap flow approach to estimate sub-daily VWC variations in corn with data from our 2019 campaign. The results confirm the possibility to estimate 15 min variations in corn VWC with only sap flow sensors and a weather station. While the indirect estimation of transpiration could be considered a drawback of the method, Fig. 6 has shown that the diurnal VWC cycle was represented generally well. In general, we found the best agreement between reconstructed and sampled VWC when

the daily cycle of transpiration was estimated from multi-day sap flow observations and  $ET_0$  estimates. Moreover, the application of CDF matching improved the reconstruction substantially on 25 July, while, on 28 August, a good agreement was already found after linear correction (Fig. 6). This difference could partly be explained by the suppressing effect that dew, observed on 25 July (Fig. 7), has on transpiration (Dawson and Goldsmith, 2018), which is not captured by  $ET_0$  (Langensiepen et al., 2009). When  $ET_0$  rates are low, estimated transpiration is lower after CDF matching than after linear correction (see Fig. 4d). Consequently, CDF matching mimicked the suppressing effect of dew due to the reduction in transpiration rates in the morning. When we look at the period between the peak of dew (06:00 LT) and full dissipation (08:15 LT) on 25 July in Fig. 6, we see that  $\Delta VWC$  is  $0.17 \text{ kg m}^{-2}$  in the second row, while  $\Delta VWC$  is  $0.1 \text{ kg m}^{-2}$  in the third row. This means that CDF matching in this case led to reduction in transpiration of  $0.07 \text{ kg m}^{-2}$ . This is comparable to the estimated dew evaporation in this period, which was  $0.09 \text{ kg m}^{-2}$  (Fig. 7). The same holds for 23 August, when we found a transpiration reduction of about  $0.18 \text{ kg m}^{-2}$  between 06:45 and 09:45 LT after CDF matching and an estimated dew evaporation of  $0.20 \text{ kg m}^{-2}$  in the same period. On 28 August, all dew had already dissipated

before sunrise and did, thus, not affect transpiration. Therefore, a reduction in transpiration rates did not improve the reconstruction of VWC. These results illustrate that the suppressing effect of dew on transpiration should be taken into account when one estimates transpiration with a weather station or flux tower.

Another effect of CDF matching was that the highest  $ET_0$  rates resulted in higher estimates of transpiration compared to those obtained using linear corrections (see Fig. 4d). This was particularly apparent under sunny conditions such as those on 25 July and 23 August. This means that transpiration rates exceeded sap flow rates for a longer period. Together with the gradual depletion of internal VWC in the morning, this led to a much better agreement and a shift in a diurnal minimum towards the afternoon. However, the poor agreement between the sampled and reconstructed VWC in the evening of 23 August could not be explained by the extreme hydrometeorological conditions, growth stage, or drought stress. Other potential contributors to the poor agreement could be unaccounted for errors in the sap flow, weather data, or samples. The cloudier conditions on 28 August (Fig. 7) could explain the small difference between linear corrections and CDF matching.

When the methodology with CDF matching was applied to the 10 d period from our 2018 campaign, the diurnal minima of reconstructed VWC matched excellently with the diurnal minima in the backscatter in most cases (Fig. 9). This could be explained by the daily dew formation and high temperatures in this period. However, discontinuities were observed between consecutive days (Fig. 8), which might be related to the temporal resolution of the observations and the estimation of transpiration fluxes. The temporal resolution of the sensor observations was 15 min. At the same time, we found phase differences between  $ET_0$  and sap flow of the order of 15–45 min, which was consistent with previous studies on corn (e.g. Langensiepen et al., 2009). Increasing the ratio between phase difference and observation resolution would increase the robustness of the method. A potential solution would therefore be to increase the temporal resolution of the sensor observations. Another potential solution is related to the estimation of transpiration fluxes. Ideally, a flux tower would be used for ET estimates through the eddy covariance method, as it is a more direct measurement and widely considered as the most accurate technique for ET measurements at field scale (Zhang et al., 2014; Maltese et al., 2018; Oguntunde et al., 2004). Improved ET estimates may also reduce or eliminate the need to include CDF matching. As direct ET measurements also include evaporation from SCW and soil, it is advised to include leaf wetness sensors and micro-lysimeters (Ding et al., 2013) to provide quantitative estimates of evaporation and determine transpiration from ET measurements. Including several in situ sensors of each type (leaf wetness, sap flow, etc.) ensures that the quantities capture field-scale dynamics.

## 5.2 Interpreting sub-daily backscatter

In Vermunt et al. (2020), sub-daily L-band backscatter variations were attributed to VWC, SCW, and soil moisture. However, the lack of sub-daily VWC data points complicated quantifying the relation between backscatter and the individual moisture stores. The VWC records generated in the current study allowed us to understand sub-daily backscatter variations with unprecedented detail and to describe the relative backscatter sensitivity to the different moisture stores.

The results presented here indicate that the effects of sub-daily variations in VWC on backscatter are considerable. Our regression analysis suggested that, on a typical dry day, the diurnal cycle of VWC led to a 2 (HH- and cross-pol) to almost 4 (VV-pol) times higher change in backscatter than the soil moisture drydown did. Note that these ratios can be different when either VWC or soil moisture content substantially change (Brisco et al., 1990) or when the crop structure changes during the day (Kimes and Kirchner, 1983). Backscatter sensitivity to VWC dynamics was most clearly observed in the period between sunrise and mid-afternoon, when both dropped significantly. During mid-afternoon to sunset, we observed a constant to slightly increasing VV- and cross-polarized backscatter, which illustrated the opposite effects of VWC refilling and soil moisture drop on backscatter. Nocturnal backscatter dynamics demonstrated the sensitivity of VV- and cross-pol to SCW.

In general, our results showed that VV-pol was more sensitive to variations in VWC than HH-pol and less sensitive to variations in soil moisture. This is in agreement with Joseph et al. (2010), who described a larger attenuation of the soil return by vegetation for VV-pol compared to HH-pol in a study on the L-band backscattering of corn. An explanation for this difference was given by Stamenković et al. (2015), who described that, at VV and HV polarizations, vertical corn stems attenuate the double-bounce scattering at L-band, which results in lower contribution from the soil. As a consequence, volume scattering and the corresponding contribution from vegetation becomes dominant. At HH-pol, there is less attenuation of the double bounce effect, which explains a higher sensitivity to soil moisture (Table 2).

Moreover, the nocturnal VV- and cross-polarized backscatter increase in Figs. 9 and 11 could be attributed to dew formation only because VWC was stable during the night, and soil moisture was constant or decreased slightly. Stable nocturnal VWC can be expected for crops with a hydraulic capacitance similar to or lower than corn and sufficient soil moisture availability. For vegetation with a larger hydraulic capacitance or low soil moisture availability, nocturnal refilling of VWC could be expected (Maltese et al., 2018), which could complicate the separation of signals from VWC and SCW.

Figures 9–11 and Table 2 showed that, compared to HH-pol, VV- and cross-polarized backscatter were not only more sensitive to changes in VWC but also to changing SCW.

This is in agreement with previous findings from Brancato et al. (2017), who found a stronger effect of SCW on S- and C-band differential interferometric observables in VV polarization compared to other polarizations, particularly for vertically oriented crops as corn. This could be related to increased scattering from wet leaves in combination with the dominance of volume scattering in VV and cross-polarizations. However, it seems that the SCW coefficients ( $c$ ) for VV- and cross-pol in Table 2 underestimate the effect of dew on backscatter, as the nocturnal increases in calculated  $\sigma_{VV}^0$  and  $\sigma_{cross}^0$  in Fig. 12 are lower than observed. This could partly be addressed by improved SCW estimates, for example, through the inclusion of more leaf wetness sensors distributed in the canopy (Vermunt et al., 2020). Moreover, additional research is needed to provide more insight into the scattering mechanisms under the presence of SCW, for example, by considering SCW in physical backscattering models.

## 6 Conclusions

The potential of using radar for (eco)hydrological studies is limited by the challenge to separate signals from soil and vegetation on a sub-daily timescale. To gain a better understanding of what controls sub-daily backscatter behaviour, we analysed tower-based polarimetric L-band observations from a cornfield using unique estimates of moisture fluctuations in vegetation and soil.

A method developed by the tree physiology community was adapted to estimate continuous variations in corn plant water content with unprecedented detail. The adaptations were related to the estimation of transpiration. The best agreement between sampled and estimated VWC was found when transpiration estimates were obtained after the removal of systematic differences between  $ET_0$  and sap flow. In non-stressed conditions, predawn VWC decreased by 10 %–20 % during the day.

Complementing the resulting record of VWC with records of soil moisture and previously estimated surface canopy water allowed us to interpret the sub-daily behaviour of polarimetric L-band observations. The results showed a significant effect of diurnal VWC cycles on L-band backscatter when the plants reached their maximum size. The highest and lowest sensitivity to VWC was found in VV- and HH-polarized backscatter, respectively. The regression results suggested that the backscatter behaviour on a typical dry day was 2 (HH- and cross-pol) to 4 (VV) times more determined by the VWC cycle than by soil moisture. Night-time increases in VV- and cross-polarized backscatter were a result of dew formation only.

The results presented here provide unique insight into the potentially confounding influence of surface and internal vegetation water content variations on backscatter, particularly in the interpretation of sub-daily radar observations. These findings are directly relevant for current and upcoming L-band missions, but also for the design of future spaceborne SAR missions for land applications. In particular, this study highlights the potential difference in relative importance of VWC, SCW, or soil moisture dynamics, depending on the overpass time. This is particularly relevant given the imminent availability of sub-daily observations from, e.g., the IC-EYE and Capella Space constellations.

As radar observations are increasingly used to study plant water status, the presented sap flow method is a promising way to validate sub-daily satellite observations with just meteorological data and sap flow sensors, without laborious sub-daily destructive sampling. The method is expected to be most robust when the temporal resolution of the sap flow and ET observations are significantly smaller than the phase difference between the two, which depends on the species. The number of sensors required to capture VWC variations at footprint scale is expected to depend on the footprint size, the spatial heterogeneity of vegetation type, and factors influencing moisture supply and demand. Potentially, global database networks for sap flow measurements, i.e. SAPFLUXNET (<http://sapfluxnet.creaf.cat>, last access: 2 June 2021), and flux tower measurements, e.g. FLUXNET (<https://fluxnet.org/>, last access: 2 June 2021) and AmeriFlux (<https://ameriflux.lbl.gov/>, last access: 2 June 2021), can play an important role here.

Moreover, the utility of the tested sap flow method goes well beyond radar remote sensing. It also has huge potential for validating and interpreting a wide range of other remote sensing techniques that are sensitive to vegetation water, such as passive microwave remote sensing, global navigation satellite systems (GNSSs), and cosmic ray neutron sensors.



## Appendix A

**Table A1.** Root mean squared error (RMSE) between reconstructed and sampled VWC. The rows represent time of constraining the reconstruction, while the columns represent the considered period for linear  $ET_0$  correction.

	25 July			23 August					28 August				
	1 d	3 d	All data	1 d	3 d	5 d	7 d	All data	1 d	3 d	5 d	7 d	All data
Predawn	0.212	0.272	1.107	0.369	0.310	0.256	0.282	0.547	0.178	0.097	0.095	0.063	0.352
Morning	0.314	0.369	1.082	0.500	0.444	0.389	0.416	0.655	0.176	0.110	0.108	0.078	0.315
Afternoon	0.187	0.220	0.704	0.375	0.346	0.318	0.331	0.468	0.129	0.090	0.089	0.075	0.227
Evening	0.266	0.321	1.036	0.446	0.392	0.337	0.364	0.601	0.206	0.138	0.136	0.106	0.351
Sunset	0.247	0.311	1.131	0.516	0.448	0.379	0.413	0.706	0.150	0.074	0.072	0.047	0.317

**Table A2.** Root mean squared error (RMSE) between reconstructed and sampled VWC. The rows represent time of constraining the reconstruction, while the columns represent the considered period for CDF matching.

	25 July			23 August					28 August				
	1 d	3 d	All data	1 d	3 d	5 d	7 d	All data	1 d	3 d	5 d	7 d	All data
Predawn	0.155	0.140	0.070	0.303	0.380	0.295	0.310	0.458	0.135	0.112	0.153	0.149	0.379
Morning	0.114	0.104	0.124	0.296	0.390	0.313	0.331	0.508	0.121	0.078	0.100	0.088	0.286
Afternoon	0.140	0.136	0.125	0.309	0.351	0.311	0.319	0.402	0.091	0.060	0.075	0.067	0.212
Evening	0.094	0.081	0.113	0.244	0.333	0.259	0.276	0.451	0.142	0.084	0.103	0.083	0.306
Sunset	0.177	0.162	0.083	0.471	0.548	0.460	0.474	0.623	0.102	0.070	0.106	0.097	0.325

**Table A3.** Offset between reconstructed and sampled VWC. The rows represent the method used for transpiration estimation, while the columns represent the considered period.

	4 Jun				8 June					11 June			
	1 d	3 d	5 d	All data	1 d	3 d	5 d	7 d	All data	1 d	3 d	5 d	All data
Linear	0.202	0.250	0.149	0.055	0.412	0.071	0.241	0.022	0.022	0.556	0.790	0.739	0.543
CDF	0.134	0.180	0.185	0.063	0.292	0.106	0.209	0.147	0.128	0.456	0.476	0.521	0.267

**Table A4.** Summary of multiple linear regression results.

	VV-pol			HH-pol			Cross-pol		
	$\theta$	VWC	SCW	$\theta$	VWC	SCW	$\theta$	VWC	SCW
Coeff.	24.0643	2.9340	0.6190	39.4680	2.2879	0.3759	38.8273	2.4463	0.7293
SE	2.600	0.262	0.302	3.019	0.304	0.350	2.906	0.293	0.337
$t$	9.254	11.203	2.051	13.075	7.526	1.073	13.363	8.360	2.163
$P >  t $	0.000	0.000	0.043	0.000	0.000	0.286	0.000	0.000	0.033
(0.025	18.900	2.414	0.020	33.474	1.684	-0.320	33.058	1.865	0.060
0.975)	29.228	3.454	1.218	45.462	2.892	1.072	44.597	3.027	1.399
$R^2$		0.686			0.690			0.715	
Adj. $R^2$		0.675			0.680			0.706	

*Code and data availability.* Meteorological data with 15 min resolution were obtained from the nearby Florida Automated Weather Network (FAWN) weather station, downloaded from the Report Generator (<https://fawn.ifas.ufl.edu/data/reports/>; FAWN, 2018).

The data from field measurements are not publicly available yet.

*Supplement.* The supplement related to this article is available online at: <https://doi.org/10.5194/hess-26-1223-2022-supplement>.

*Author contributions.* PV, SSD, and NvdG were responsible for the conceptualization, methodology, formal analysis, investigation, visualization, and writing (original draft preparation). JJ provided resources (scatterometer data). PV and SK conducted the ground measurements. SSD and NvdG provided supervision. All authors contributed to writing (review and editing).

*Competing interests.* The contact author has declared that neither they nor their co-authors have any competing interests.

*Disclaimer.* Publisher's note: Copernicus Publications remains neutral with regard to jurisdictional claims in published maps and institutional affiliations.

*Acknowledgements.* The experiment in 2018 was made possible by infrastructural and technical support from the Agricultural and Biological Engineering Department and PSREU at the University of Florida. The authors wish to acknowledge the help from Daniel Preston, Patrick Rush, Eduardo Carrascal, and James Boyer and his team in particular. The experiment in 2019 was made possible by infrastructural and technical support from Jacob van den Borne, Paul van Zoggel, and their team. Vineet Kumar participated in the collection of field data in 2019.

*Financial support.* This project was supported by the Vidi Grant 14126 from the Dutch Technology Foundation STW, which is part of The Netherlands Organisation for Scientific Research (NWO) and which is partly funded by the Ministry of Economic Affairs.

*Review statement.* This paper was edited by Alexander Gruber and reviewed by Andrew Feldman and two anonymous referees.

## References

Allen, R. G., Pereira, L. S., Raes, D., and Smith, M.: Crop evapotranspiration: guidelines for computing crop water requirements, FAO Drainage and Irrigation Paper 56, Tech. rep., FAO – Food and Agriculture Organization of the United Nations, Rome, 1998.

- Bartholomeus, R., de Louw, P., Witte, F., van Dam, J., van Deijl, D., Hoefsloot, P., van Huijgevoort, M., Hunink, J., America, I., Pouwels, J., and de Wit, J.: Droogte in zandgebieden van Zuid-, Midden-en Oost-Nederland: Het verhaal: analyse van droogte 2018 en 2019 en tussentijdse bevindingen, Tech. rep., KWR, <https://edepot.wur.nl/534198> (last access: 13 August 2021), 2020.
- Bracaglia, M., Ferrazzoli, P., and Guerriero, L.: A fully polarimetric multiple scattering model for crops, *Remote Sens. Environ.*, 54, 170–179, [https://doi.org/10.1016/0034-4257\(95\)00151-4](https://doi.org/10.1016/0034-4257(95)00151-4), 1995.
- Brancato, V., Liebisch, F., and Hajnsek, I.: Impact of Plant Surface Moisture on Differential Interferometric Observables: A Controlled Electromagnetic Experiment, *IEEE T. Geosci. Remote.*, 55, 3949–3964, <https://doi.org/10.1109/TGRS.2017.2684814>, 2017.
- Brisco, B., Brown, R. J., Koehler, J. A., Sofko, G. J., and McKibben, M. J.: The diurnal pattern of microwave backscattering by wheat, *Remote Sens. Environ.*, 34, 37–47, [https://doi.org/10.1016/0034-4257\(90\)90082-W](https://doi.org/10.1016/0034-4257(90)90082-W), 1990.
- Brocca, L., Hasenauer, S., Lacava, T., Melone, F., Moramarco, T., Wagner, W., Dorigo, W., Matgen, P., Martínez-Fernández, J., Llorens, P., Latron, J., Martin, C., and Bittelli, M.: Soil moisture estimation through ASCAT and AMSR-E sensors: An intercomparison and validation study across Europe, *Remote Sens. Environ.*, 115, 3390–3408, <https://doi.org/10.1016/j.rse.2011.08.003>, 2011.
- Cosh, M. H., Kabela, E. D., Hornbuckle, B., Gleason, M. L., Jackson, T. J., and Prueger, J. H.: Observations of dew amount using in situ and satellite measurements in an agricultural landscape, *Agr. Forest Meteorol.*, 149, 1082–1086, <https://doi.org/10.1016/j.agrformet.2009.01.004>, 2009.
- Cosh, M. H., Ochsner, T. E., McKee, L., Dong, J., Basara, J. B., Evett, S. R., Hatch, C. E., Small, E. E., Steele-Dunne, S. C., Zreda, M., and Sayde, C.: The Soil Moisture Active Passive Marena, Oklahoma, In Situ Sensor Testbed (SMAP-MOISS): Testbed Design and Evaluation of In Situ Sensors, *Vadose Zone J.*, 15, 1–11, <https://doi.org/10.2136/vzj2015.09.0122>, 2016.
- Čermák, J., Kučera, J., Bauerle, W. L., Phillips, N., and Hinckley, T. M.: Tree water storage and its diurnal dynamics related to sap flow and changes in stem volume in old-growth Douglas-fir trees, *Tree Physiol.*, 27, 181–198, <https://doi.org/10.1093/treephys/27.2.181>, 2007.
- Dawson, T. E. and Goldsmith, G. R.: The value of wet leaves, *New Phytol.*, 219, 1156–1169, <https://doi.org/10.1111/nph.15307>, 2018.
- Ding, R., Kang, S., Zhang, Y., Hao, X., Tong, L., and Du, T.: Partitioning evapotranspiration into soil evaporation and transpiration using a modified dual crop coefficient model in irrigated maize field with ground-mulching, *Agricult. Water Manage.*, 127, 85–96, <https://doi.org/10.1016/j.agwat.2013.05.018>, 2013.
- Dobriyal, P., Qureshi, A., Badola, R., and Hussain, S. A.: A review of the methods available for estimating soil moisture and its implications for water resource management, *J. Hydrol.*, 458–459, 110–117, <https://doi.org/10.1016/j.jhydrol.2012.06.021>, 2012.
- Drusch, M., Wood, E. F., and Gao, H.: Observation operators for the direct assimilation of TRMM microwave imager retrieved soil moisture, *Geophys. Res. Lett.*, 32, L15403, <https://doi.org/10.1029/2005GL023623>, 2005.

- El Hajj, M., Baghdadi, N., Wigneron, J.-P., Zribi, M., Albergel, C., Calvet, J.-C., and Fayad, I.: First Vegetation Optical Depth Mapping from Sentinel-1 C-band SAR Data over Crop Fields, *Remote Sens.*, 11, 2769, <https://doi.org/10.3390/rs11232769>, 2019.
- Emmerik, T. V., Steele-Dunne, S. C., Judge, J., and v. d. Giesen, N.: Impact of Diurnal Variation in Vegetation Water Content on Radar Backscatter From Maize During Water Stress, *IEEE T. Geosci. Remote*, 53, 3855–3869, <https://doi.org/10.1109/TGRS.2014.2386142>, 2015.
- Emmerik, T. V., Steele-Dunne, S., Paget, A., Oliveira, R. S., Bitencourt, P. R. L., Barros, F. D. V., and v. d. Giesen, N.: Water stress detection in the Amazon using radar, *Geophys. Res. Lett.*, 44, 6841–6849, <https://doi.org/10.1002/2017GL073747>, 2017.
- Entekhabi, D., Njoku, E. G., O'Neill, P. E., Kellogg, K. H., Crow, W. T., Edelstein, W. N., Entin, J. K., Goodman, S. D., Jackson, T. J., Johnson, J., Kimball, J., Piepmeier, J. R., Koster, R. D., Martin, N., McDonald, K. C., Moghaddam, M., Moran, S., Reichle, R., Shi, J. C., Spencer, M. W., Thurman, S. W., Tsang, L., and Zyl, J. V.: The Soil Moisture Active Passive (SMAP) Mission, *Proc. IEEE*, 98, 704–716, <https://doi.org/10.1109/JPROC.2010.2043918>, 2010.
- Farquharson, G., Castelletti, D., Stringham, C., and Eddy, D.: An Update on the Capella Space Radar Constellation, in: *EU-SAR 2021; 13th European Conference on Synthetic Aperture Radar*, 29 March–1 April 2021, online, 1–4, 2021.
- FAWN: Report Generator, <https://fawn.ifas.ufl.edu/data/reports/>, last access: 10 October 2018.
- Frolking, S., Milliman, T., Palace, M., Wisser, D., Lammers, R., and Fahnestock, M.: Tropical forest backscatter anomaly evident in SeaWinds scatterometer morning overpass data during 2005 drought in Amazonia, *Remote Sens. Environ.*, 115, 897–907, <https://doi.org/10.1016/j.rse.2010.11.017>, 2011.
- Goldstein, G., Andrade, J. L., Meinzer, F. C., Holbrook, N. M., Cavellier, J., Jackson, P., and Celis, A.: Stem water storage and diurnal patterns of water use in tropical forest canopy trees, *Plant Cell Environ.*, 21, 397–406, <https://doi.org/10.1046/j.1365-3040.1998.00273.x>, 1998.
- Hamadi, A., Albinet, C., Borderies, P., Koleck, T., Villard, L., Ho Tong Minh, D., and Le Toan, T.: Temporal Survey of Polarimetric P-Band Scattering of Tropical Forests, *IEEE T. Geosci. Remote*, 52, 4539–4547, <https://doi.org/10.1109/TGRS.2013.2282357>, 2014.
- Ignatenko, V., Laurila, P., Radius, A., Lamentowski, L., Antropov, O., and Muff, D.: ICEYE Microsatellite SAR Constellation Status Update: Evaluation of First Commercial Imaging Modes, in: *IGARSS – IEEE International Geoscience and Remote Sensing Symposium*, Online, 3581–3584, <https://doi.org/10.1109/IGARSS39084.2020.9324531>, 2020.
- Joseph, A. T., van der Velde, R., O'Neill, P. E., Lang, R., and Gish, T.: Effects of corn on C- and L-band radar backscatter: A correction method for soil moisture retrieval, *Remote Sens. Environ.*, 114, 2417–2430, <https://doi.org/10.1016/j.rse.2010.05.017>, 2010.
- Kim, S.-B., v. Zyl, J. J., Johnson, J. T., Moghaddam, M., Tsang, L., Colliander, A., Dunbar, R. S., Jackson, T. J., Jaruwatanadilok, S., West, R., Berg, A., Caldwell, T., Cosh, M. H., Goodrich, D. C., Livingston, S., López-Baeza, E., Rowlandson, T., Thibeault, M., Walker, J. P., Entekhabi, D., Njoku, E. G., O'Neill, P. E., and Yueh, S. H.: Surface Soil Moisture Retrieval Using the L-Band Synthetic Aperture Radar Onboard the Soil Moisture Active–Passive Satellite and Evaluation at Core Validation Sites, *IEEE T. Geosci. Remote*, 55, 1897–1914, <https://doi.org/10.1109/TGRS.2016.2631126>, 2017.
- Kimes, D. S. and Kirchner, J. A.: Diurnal variations of vegetation canopy structure, *Int. J. Remote Sens.*, 4, 257–271, <https://doi.org/10.1080/01431168308948545>, 1983.
- Köcher, P., Horna, V., and Leuschner, C.: Stem water storage in five coexisting temperate broad-leaved tree species: significance, temporal dynamics and dependence on tree functional traits, *Tree Physiol.*, 33, 817–832, <https://doi.org/10.1093/treephys/tpt055>, 2013.
- Konings, A. G., Yu, Y., Xu, L., Yang, Y., Schimel, D. S., and Saatchi, S. S.: Active microwave observations of diurnal and seasonal variations of canopy water content across the humid African tropical forests, *Geophys. Res. Lett.*, 44, 2290–2299, <https://doi.org/10.1002/2016GL072388>, 2017.
- Konings, A. G., Rao, K., and Steele-Dunne, S. C.: Macro to micro: microwave remote sensing of plant water content for physiology and ecology, *New Phytol.*, 223, 1166–1172, <https://doi.org/10.1111/nph.15808>, 2019.
- Konings, A. G., Saatchi, S. S., Frankenberg, C., Keller, M., Leshyk, V., Anderegg, W. R. L., Humphrey, V., Matheny, A. M., Trugman, A., Sack, L., Agee, E., Barnes, M. L., Binks, O., Cawse-Nicholson, K., Christoffersen, B. O., Entekhabi, D., Gentine, P., Holtzman, N. M., Katul, G. G., Liu, Y., Longo, M., Martinez-Vilalta, J., McDowell, N., Meir, P., Mencuccini, M., Mrad, A., Novick, K. A., Oliveira, R. S., Siqueira, P., Steele-Dunne, S. C., Thompson, D. R., Wang, Y., Wehr, R., Wood, J. D., Xu, X., and Zuidema, P. A.: Detecting forest response to droughts with global observations of vegetation water content, *Global Change Biol.*, 27, 6005–6024, <https://doi.org/10.1111/gcb.15872>, 2021.
- Langensiepen, M., Fuchs, M., Bergamaschi, H., Moreshet, S., Cohen, Y., Wolff, P., Jutzi, S. C., Cohen, S., Rosa, L. M. G., Li, Y., and Fricke, T.: Quantifying the uncertainties of transpiration calculations with the Penman–Monteith equation under different climate and optimum water supply conditions, *Agr. Forest Meteorol.*, 149, 1063–1072, <https://doi.org/10.1016/j.agrformet.2009.01.001>, 2009.
- Maltese, A., Awada, H., Capodici, F., Ciralo, G., La Loggia, G., and Rallo, G.: On the Use of the Eddy Covariance Latent Heat Flux and Sap Flow Transpiration for the Validation of a Surface Energy Balance Model, *Remote Sens.*, 10, 195, <https://doi.org/10.3390/rs10020195>, 2018.
- Meinzer, F. C., James, S. A., and Goldstein, G.: Dynamics of transpiration, sap flow and use of stored water in tropical forest canopy trees, *Tree Physiol.*, 24, 901–909, <https://doi.org/10.1093/treephys/24.8.901>, 2004.
- Monteith, A. R. and Ulander, L. M. H.: Temporal Characteristics of P-Band Tomographic Radar Backscatter of a Boreal Forest, *IEEE J. Select. Top. Appl. Earth Obs. Remote Sens.*, 14, 1967–1984, <https://doi.org/10.1109/JSTARS.2021.3050611>, 2021.
- Nagarajan, K., Liu, P., DeRoo, R., Judge, J., Akbar, R., Rush, P., Feagle, S., Preston, D., and Terwilliger, R.: Automated L-Band Radar System for Sensing Soil Moisture at High Temporal Resolution, *IEEE Geosci. Remote Sens. Lett.*, 11, 504–508, <https://doi.org/10.1109/LGRS.2013.2270453>, 2014.
- Oguntunde, P. G., v. d. Giesen, N. C., Vlek, P. L. G., and Eggers, H.: Water Flux in a Cashew Orchard during a Wet-to-Dry Tran-

- sition Period: Analysis of Sap Flow and Eddy Correlation Measurements, *Earth Interact.*, 8, 1–17, [https://doi.org/10.1175/1087-3562\(2004\)8<1:WFIACO>2.0.CO;2](https://doi.org/10.1175/1087-3562(2004)8<1:WFIACO>2.0.CO;2), 2004.
- Paget, A. C., Long, D. G., and Madsen, N. M.: RapidScat Diurnal Cycles Over Land, *IEEE T. Geosci. Remote*, 54, 3336–3344, <https://doi.org/10.1109/TGRS.2016.2515022>, 2016.
- Phillips, N. G., Scholz, F. G., Bucci, S. J., Goldstein, G., and Meinzer, F. C.: Using branch and basal trunk sap flow measurements to estimate whole-plant water capacitance: comment on Burgess and Dawson (2008), *Plant Soil*, 315, 315–324, <https://doi.org/10.1007/s11104-008-9741-y>, 2008.
- Pierdicca, N., Davidson, M., Chini, M., Dierking, W., Djavidnia, S., Haarpaintner, J., Hajduch, G., Laurin, G. V., Laval, M., López-Martínez, C., Nagler, T., and Su, B.: The Copernicus L-band SAR mission ROSE-L (Radar Observing System for Europe) (Conference Presentation), in: *Active and Passive Microwave Remote Sensing for Environmental Monitoring III*, vol. 11154, International Society for Optics and Photonics, p. 111540E, <https://doi.org/10.1117/12.2534743>, 2019.
- Quegan, S., Le Toan, T., Chave, J., Dall, J., Exbrayat, J.-F., Minh, D. H. T., Lomas, M., D'Alessandro, M. M., Pailou, P., Papathanassiou, K., Rocca, F., Saatchi, S., Scipal, K., Shugart, H., Smallman, T. L., Soja, M. J., Tebaldini, S., Ulander, L., Villard, L., and Williams, M.: The European Space Agency BIOMASS mission: Measuring forest above-ground biomass from space, *Remote Sens. Environ.*, 227, 44–60, <https://doi.org/10.1016/j.rse.2019.03.032>, 2019.
- Rafi, Z., Merlin, O., Le Dantec, V., Khabba, S., Mordelet, P., Er-Raki, S., Amazirh, A., Olivera-Guerra, L., Ait Hsaine, B., Simonneaux, V., Ezzahar, J., and Ferrer, F.: Partitioning evapotranspiration of a drip-irrigated wheat crop: Inter-comparing eddy covariance-, sap flow-, lysimeter- and FAO-based methods, *Agr. Forest Meteorol.*, 265, 310–326, <https://doi.org/10.1016/j.agrformet.2018.11.031>, 2019.
- Reichle, R. H. and Koster, R. D.: Bias reduction in short records of satellite soil moisture, *Geophys. Res. Lett.*, 31, L19501, <https://doi.org/10.1029/2004GL020938>, 2004.
- Rosen, P. A., Kim, Y., Kumar, R., Misra, T., Bhan, R., and Sagi, V. R.: Global persistent SAR sampling with the NASA-ISRO SAR (NISAR) mission, in: 2017 IEEE Radar Conference (RadarConf), 0410–0414, <https://doi.org/10.1109/RADAR.2017.7944237>, iSSN: 2375-5318, 2017.
- Sakuratani, T.: A Heat Balance Method for Measuring Water Flux in the Stem of Intact Plants, *J. Agricult. Meteorol.*, 37, 9–17, <https://doi.org/10.2480/agrmet.37.9>, 1981.
- Schroeder, R., McDonald, K. C., Azarderakhsh, M., and Zimmermann, R.: ASCAT MetOp-A diurnal backscatter observations of recent vegetation drought patterns over the contiguous U.S.: An assessment of spatial extent and relationship with precipitation and crop yield, *Remote Sens. Environ.*, 177, 153–159, <https://doi.org/10.1016/j.rse.2016.01.008>, 2016.
- Stamenković, J., Ferrazzoli, P., Guerriero, L., Tuia, D., and Thiran, J.-P.: Joining a Discrete Radiative Transfer Model and a Kernel Retrieval Algorithm for Soil Moisture Estimation From SAR Data, *IEEE J. Select. Top. Appl. Earth Obs. Remote Sens.*, 8, 3463–3475, <https://doi.org/10.1109/JSTARS.2015.2432854>, 2015.
- Steele-Dunne, S. C., Friesen, J., and van de Giesen, N.: Using Diurnal Variation in Backscatter to Detect Vegetation Water Stress, *IEEE T. Geosci. Remote*, 50, 2618–2629, <https://doi.org/10.1109/TGRS.2012.2194156>, 2012.
- Steele-Dunne, S. C., McNairn, H., Monsivais-Huertero, A., Judge, J., Liu, P.-W., and Papathanassiou, K.: Radar Remote Sensing of Agricultural Canopies: A Review, *IEEE J. Select. Top. Appl. Earth Obs. Remote Sens.*, 10, 2249–2273, <https://doi.org/10.1109/JSTARS.2016.2639043>, 2017.
- Steele-Dunne, S. C., Hahn, S., Wagner, W., and Vreugdenhil, M.: Investigating vegetation water dynamics and drought using Metop ASCAT over the North American Grasslands, *Remote Sens. Environ.*, 224, 219–235, <https://doi.org/10.1016/j.rse.2019.01.004>, 2019.
- Swanson, R. H.: Significant historical developments in thermal methods for measuring sap flow in trees, *Agr. Forest Meteorol.*, 72, 113–132, [https://doi.org/10.1016/0168-1923\(94\)90094-9](https://doi.org/10.1016/0168-1923(94)90094-9), 1994.
- Thompson, A. A.: Overview of the RADARSAT Constellation Mission, *Can. J. Remote Sens.*, 41, 401–407, <https://doi.org/10.1080/07038992.2015.1104633>, 2015.
- Torres, R., Snoeij, P., Geudtner, D., Bibby, D., Davidson, M., Attema, E., Potin, P., Rommen, B., Floury, N., Brown, M., Traver, I. N., Deghaye, P., Duesmann, B., Rosich, B., Miranda, N., Bruno, C., L'Abbate, M., Croci, R., Pietropaolo, A., Huchler, M., and Rostan, F.: GMES Sentinel-1 mission, *Remote Sens. Environ.*, 120, 9–24, <https://doi.org/10.1016/j.rse.2011.05.028>, 2012.
- Vermunt, P. C., Khabbazan, S., Steele-Dunne, S. C., Judge, J., Monsivais-Huertero, A., Guerriero, L., and Liu, P.-W.: Response of Subdaily L-Band Backscatter to Internal and Surface Canopy Water Dynamics, *IEEE T. Geosci. Remote*, 59, 7322–7337, <https://doi.org/10.1109/TGRS.2020.3035881>, 2020.
- Vreugdenhil, M., Wagner, W., Bauer-Marschallinger, B., Pfeil, I., Teubner, I., Rüdiger, C., and Strauss, P.: Sensitivity of Sentinel-1 Backscatter to Vegetation Dynamics: An Austrian Case Study, *Remote Sens.*, 10, 1396, <https://doi.org/10.3390/rs10091396>, 2018.
- Xu, X., Konings, A. G., Longo, M., Feldman, A., Xu, L., Saatchi, S., Wu, D., Wu, J., and Moorcroft, P.: Leaf surface water, not plant water stress, drives diurnal variation in tropical forest canopy water content, *New Phytol.*, 231, 122–136, <https://doi.org/10.1111/nph.17254>, 2021.
- Ye, N., Walker, J. P., Wu, X., de Jeu, R., Gao, Y., Jackson, T. J., Jonard, F., Kim, E., Merlin, O., Pauwels, V. R. N., Renzullo, L. J., Rüdiger, C., Sabaghy, S., von Hebel, C., Yueh, S. H., and Zhu, L.: The Soil Moisture Active Passive Experiments: Validation of the SMAP Products in Australia, *IEEE T. Geosci. Remote*, 59, 2922–2939, <https://doi.org/10.1109/TGRS.2020.3007371>, 2021.
- Zhang, Z., Tian, F., Hu, H., and Yang, P.: A comparison of methods for determining field evapotranspiration: photosynthesis system, sap flow, and eddy covariance, *Hydrol. Earth Syst. Sci.*, 18, 1053–1072, <https://doi.org/10.5194/hess-18-1053-2014>, 2014.
- Zotarelli, L., Dukes, M. D., Romero, C. C., Migliaccio, K. W., and Morgan, K.: Step by Step Calculation of the Penman-Monteith Evapotranspiration (FAO-56 method), Institute of Food and Agricultural Sciences, University of Florida, Florida, USA, <https://edis.ifas.ufl.edu/pdf/FILES/AE/AE45900.pdf> (last access: 9 June 2021), 2010.